2-1-2007

Numerical modeling of concrete masonry walls strengthened by fiber reinforced polymers under lateral loads

Mohamed Salama

The American University in Cairo
School of Sciences and Engineering
Interdisciplinary Engineering Programs

NUMERICAL MODELING OF CONCRETE MASONRY WALLS STRENGTHENED BY FIBER REINFORCED POLYMERS UNDER LATERAL LOADS

BY

Mohamed Amr Salama

A thesis submitted in partial fulfillment of the requirements for the degree of

Master of Science in Engineering

with specialization in:

Construction Engineering

under the supervision of:

Dr. Medhat A. Haroun
Dean and AGIP Professor
School of Sciences and Engineering

Summer 2006

TABLE OF CONTENTS

LIST OF FIGURES

LIST OF TABLES

ACKNOWLEDGMENT

I gratefully acknowledge the support of Dr. Medhat Haroun (my advisor) for his effort in guiding me throughout my master's degree. He has always been an excellent tutor and professor, which helped me to learn so much.

I want also to express my deepest gratitude for my parents and future wife for their love and support during this research.

Last but not least I want to thank any person who helped me in my thesis or even tried, because it really made a difference.

ABSTRACT

NUMERICAL MODELING OF CONCRETE MASONRY WALLS STRENGTHENED BY FIBER REINFORCED POLYMERS UNDER LATERAL LOADS

by

Mohamed Amr Salama

In Partial Fulfillment of the Master of Science Degree in Engineering

(Construction Engineering)

Summer 2006

Professor Medhat A. Haroun, Chair

The use of fiber reinforced polymers (FRP) for the seismic retrofit of masonry walls is on the rise. Design formulae are available to estimate the lateral load capacity of the strengthened walls. However, recent experimental data from tests conducted on full-scale concrete masonry walls under cyclic lateral loads have shown that these design capacities have not been reached because of the occurrence of other failure modes not accounted for in the design formulae. The limiting failure mode in all test samples referred to in this work was due to premature compression failure of the masonry units at the wall toe.

The main goal of the current study is to develop a simple numerical model that can be readily used by practicing engineers to predict accurate levels of design capacities for strengthened masonry walls subjected to lateral loading. The numerical model needs only be sophisticated enough to provide the necessary basic information required for

design purposes. A simple and efficient finite element model of the masonry wall was devised using the software package ABACUS/STANDARD. In particular, the model uses a layered shell element which allows the modeling of the masonry in addition to the FRP laminates or strips. The analysis is performed under constant vertical gravity load with monotonically increased lateral load until wall failure. Appropriate mesh sizes, boundary conditions, restraints, modeling of steel reinforcement, and the no-compression criterion for the laminates are evaluated and their effects are illustrated. Finally, a comparison between the numerical lateral loads at failure of the walls with those observed experimentally, for the different strengthening models that were tested in the laboratory, is made. Having confirmed the validity of the theoretical model, other FRP retrofit techniques are also investigated.

The simple finite element model provided lateral capacities, for the investigated type and configuration of the masonry walls, which are most consistent with the experimentally observed values, yet significantly lower than predicted by the design formulae currently in use by practicing engineers.

CHAPTER 1

INTRODUCTION

1.1 Background

The use of Fiber Reinforced Polymers (FRP) in the building construction has become more common in the past few years. This is due to the fact that they have become cost effective, contrary to the common belief which is based on the expensive unit cost of these materials. Moreover, they have been successfully used in the repair and retrofit of concrete and masonry members that need strengthening.

FRP composites are made by mixing fibers and resins at specific volume ratio to achieve desirable properties whilst retaining each constituent's original properties. The fibers are the primary load carrying component, whilst the resin provides a continuous medium protecting the fiber reinforcement and transferring stresses between fibers. The common fibers used in composites for civil engineering applications are carbon, aramid and glass. Commonly used resins are polyester, epoxy, vinyl ester, and phenol. FRP have higher strength and lower weight compared to steel and concrete.

1.2 Problem Statement

The main causes of failure of masonry walls are the creations of excessive tensile and shearing stresses in the walls. Different types of modes of failure and damages that may occur to masonry walls are listed below:

1. Stiff wall attracting large seismic inertia forces
2. Low tensile strength of the wall (due to poor mortars)

3. Low shear strength of the wall

4. Brittle behavior in tension and compression

There exists in the literature, a large number of references to theoretical and experimental studies of the behavior of masonry walls under lateral seismic forces (shear in-plane forces). These studies vary from being elementary or limited in scope to very sophisticated numerical models or experimental test setups. Design formulas are also available to evaluate the expected strength gains when a strengthening method is used.

In 2002, Allam reported on an experimental testing of large scale walls constructed from concrete masonry blocks. These walls were retrofitted by fiber reinforced polymers and tested under lateral cyclic loads. The walls showed, in general, a much smaller resistance to lateral loads than predicted by available design equations. This is due to the occurrence of a failure mode represented by the crushing of the concrete blocks at the toe of the wall; a mode that is not taken into consideration in the design equations.

1.3 Work Objectives

Given the observed failure of strengthened walls under significantly less lateral loads than predicted by design equations, *the main goal of this study is to develop a simple numerical model that may be readily used by practicing engineers to predict accurate levels of design forces of masonry walls under lateral loading.* The numerical model should be sophisticated enough to only provide the necessary information needed for the design. Therefore, the objectives of this study are:

- To compare the theoretical (numerical) performance and modes of failure of the tested walls after being strengthened by FRP laminates with the experimentally

observed performance. In this regard, it is important to verify the lower level of ultimate lateral forces that the wall can withstand.

- To examine the validity of available design equations in predicting the shear capacity of FRP strengthened walls, through a comparison with the results of experimental tests.
- To theoretically evaluate the performance improvement of masonry walls retrofitted by other types of FRP strengthening methods.

1.4 Scope of Work

To achieve the objectives outlined in the past section, the following step-by-step procedure was adopted. In Chapter (2), a comprehensive review of the literature is presented. In particular, the experimental program, on which this study is based, was detailed with the main features of the tests and the observed results.

Chapter (3) presents the predicted lateral forces from the equations adopted by the widely-used ICBO-ES document. These formulas show a significant over strength of the walls under lateral load. The remainder of this chapter concentrates on simple analytical models that may provide an explanation for the lower capacity level of the walls as compared with the predictions from the design formulae.

In Chapter (4), the basic tools for constructing the finite element model are presented. These covered the selection of the element types, in particular, the layered shell element which allows the modeling of the wall in addition to the FRP laminates or strips. The most appropriate mesh size to predict accurate results is investigated, and the selection of a non-uniform mesh with refinements in the critical zones is also discussed. The analysis is performed under constant vertical load with monotonically increased lateral load until the wall fails. Boundary conditions, restraints, modeling

of steel reinforcement and the no-compression criterion for the laminates are also discussed. The remainder of this chapter is devoted to numerical results illustrating the effects of the previous modeling techniques and parameters.

Chapter (5) presents a comparison between the numerical loads at failure of the walls with those observed experimentally for the different strengthening models that were tested in the laboratory. Having confirmed the validity of the theoretical model, other retrofit models were also investigated.

In Chapter (6), concluding remarks are presented on the validity of this simple numerical model for predicting the wall capacity. The results are most consistent with the experimentally observed values, yet significantly lower than predicted by the design formulae for most studied cases.

CHAPTER 2

LITERATURE REVIEW

2.1 Reinforced and Unreinforced Masonry Walls under In-Plane Loading

Several research studies have been made on in-plane (shear) structural behavior of both reinforced and unreinforced masonry (URM) walls. For example, Shing et al (1989) experimentally evaluated the seismic resistance of story-height reinforced masonry shear walls. He examined the influence of the applied axial stress and the amount of vertical and horizontal reinforcement on the lateral resistance, failure mechanism, ductility and energy-dissipation capability of a wall panel. The shear strength, which is dominated by diagonal cracking, increases with the amount of vertical and horizontal steel, as well as with the tensile strength of masonry and the applied axial stress. However, the axial stress has a more significant influence on the flexural strength than on the shear strength. Furthermore, increasing the amount of vertical and horizontal reinforcement can substantially improve the post cracked ductility and energy dissipation capability of a shear specimen.

Tomazevic and Weiss (1994) studied the seismic behavior of two three- story, plain and reinforced masonry building models with identical structural configuration. The measured response and observed mechanism of the structural behavior have been used to analyze the load-bearing and energy-dissipation capacity of each structural type. They reached a conclusion that, if the walls are not reinforced, the flexural capacity of their sections below and above the slab is too low to activate the flexural capacity of horizontal structural elements. Cracks between walls and slabs occur, indicating the pier action of the walls and story mechanism of the building at the

ultimate state. If reinforced, the structural walls behave like vertical cantilevers, coupled with horizontal structural elements. The distribution of bending moments induced in the walls by seismic loads depends on the rigidity of the walls and horizontal elements.

Tomazevic et al. (1996) studied the influence of four different lateral displacement patterns on the seismic behavior of masonry walls. These patterns are:

- Monotonically increased displacements [Figure 2.1(a)]
- Cyclic lateral displacements with amplitudes, increasing in three different blocks and repeated three times at each amplitude peak [Figure 2.1(b)]
- Cyclic lateral displacements with uniformly increasing amplitudes, repeated three times at each amplitude peak, with decreasing amplitude between two consecutive blocks [Figure 2.1(c)]
- Simulated displacement response of a masonry building to an earthquake [Figure 2.1(d)]

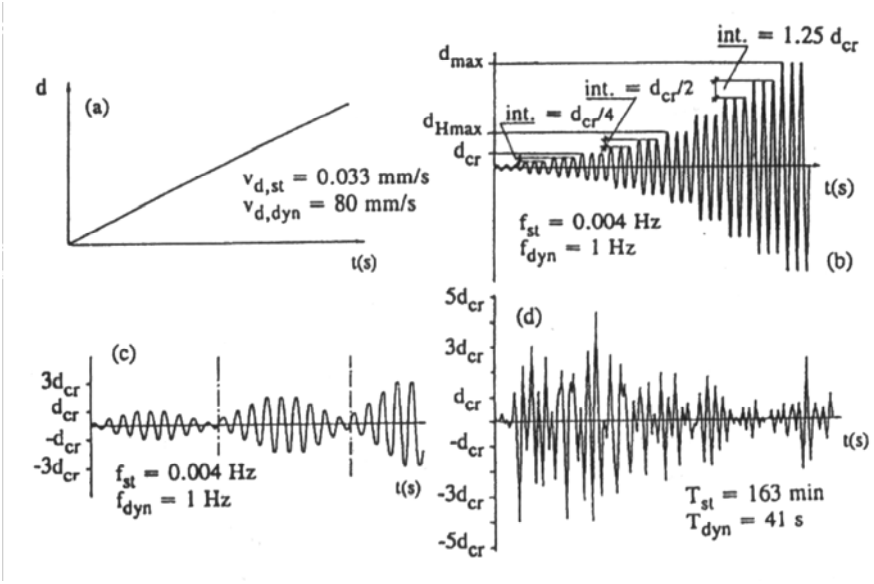

Figure (2.1) Displacement time histories used to drive actuator

(a) Monotonic; (b) Cyclic type B; (c) Cyclic type C;

(d) Simulated earthquake response

After applying these types of loads, they found out that higher resistance and larger ultimate displacements have been obtained by monotonic than by cyclic loading procedures of all types. At a higher level of vertical load, lateral resistance of the wall was improved, but deformability and ductility decreased at both static and dynamic types of loading at all load patterns.

Khalaf et al. (1994) studied the effects of the strength of concrete infill and mortar joint type on the compressive strength and behavior of unfilled and filled full and half-block prisms compressed normal to the bed face. They reached the following conclusions:

- The strength of both the full- and half-single-block-high specimens increased as the strength of the concrete infill increased.
- The presence of concrete infill significantly reduced the compressive strength of both full- and half-block prisms, with mortar joints or with plaster joints, compared to values for unfilled prisms. With only one exception, the best compressive strength results were achieved when the deformation characteristics of the infill matched those of the concrete block. This was achieved by using concrete infill with a cube compressive strength of 45 to 50 percent higher than that of the concrete block.
- Removing the mortar joint produces a large reduction in filled prism strength (a 10-mm polystyrene joint was used instead). Based on the gross area of the prism with polystyrene joint, the contribution of the concrete infill to the strength of full- and half-block prisms was found to be 25 percent.

2.2 Reinforced and Unreinforced Masonry Walls Repaired or Retrofitted by Composites under In-Plane Loading

2.2.1 Static Loading

El-hashimy et al (1997) studied the shear behavior, the deformational shapes and the load carrying capacity of ten grouted partially reinforced masonry shear walls. These walls were repaired using GRP. The walls considered were of different cross sectional shape T section, L section and rectangular walls. The repaired walls were initially loaded to failure prior to repairing them, and then the walls were retested in the same way after repairing with GRP. Different parameters were investigated as wall aspect ratio, axial stress, wall flange width and effect of repairing walls with GRP on wall reinforcement.

The conclusions reached in this study were:

- The GRP laminate is considered an efficient repair technique for damaged reinforced masonry walls because it prevented the occurrence of the original shear and splitting failures.
- The load carrying capacity of the repaired walls exceeded that of the plain walls.
- The GRP laminates decreased dramatically the internal deformations of the repaired walls.
- The GRP laminates changed the failure mode of the repaired walls from shear mode of failure to rocking mode of failure with vertical steel reinforcement yielding, which shows the efficiency of the GRP in allowing large deformations to occur without failure of the wall.
- GRP is considered an efficient repairing method for increasing the load bearing capacity and ductility of reinforced masonry walls.

Ehsani et al. (1997) studied the shear behavior of unreinforced masonry retrofitted with FRP overlays. The study included 37 clay brick specimens with FRP overlays. Three different fabric densities were used and the fiber orientation as well as the fabric length was varied to observe their effect on the developed strength. Two modes of failure were observed: (1) shear failure along the bed joint [Figure 2.2]; and (2) delamination of fabric at the middle-brick region or fabric edges. The type of failure was influenced by the fabric strength. The strength and stiffness of the specimens were highly influenced by the fiber orientation. Changing the fiber orientation from 90° to 45° led to a slight increase in the ultimate load.

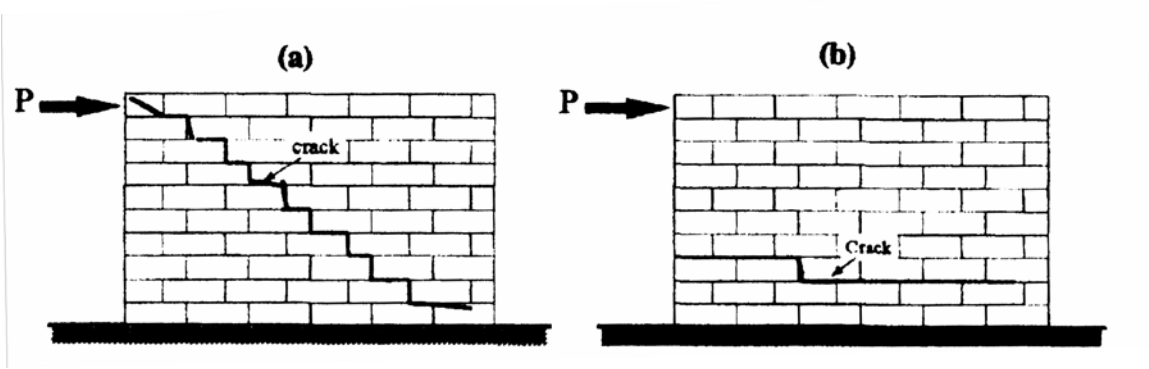

Figure (2.2) Modes of failure in URM wall subjected to lateral load P

(a) Diagonal tension; (b) Slip along bed joint

Avramidou et al. (1999) studied the strengthening against damage of brick walls by yarn composites. In this study 20 experimental specimens were prepared. The specimens had dimensions: 250mm x1140mm x 1500mm (height). Eight wall specimens were not reinforced and were used either as reference walls or for remedy after damage. The rest of the experimental specimens were reinforced by strips from yarn composites with epoxy matrix, in one case with polymer-silicate matrix (a special polymer mortar). Several types of fabrics were used with different filaments. The strips were applied in several layers (from this the thickness follows). The

reinforcing strips were glued on the walls in diagonal directions. Finally a conclusion was reached that the strengthening improved the maximum load carrying capacity of the walls and improved the deformation development.

2.2.2 Cyclic Loading

Fam et al. (2002) studied the performance of a masonry wall repaired with GFRP sheets. The original reinforced clay brick masonry wall was tested under in-plane lateral cyclic loading. Failure occurred due to yielding of the steel reinforcement and crushing of the bricks. After epoxy injection of the cracks and patching of the missing portions, the wall was repaired using GFRP sheets, applied in the horizontal and vertical directions, on one face of the wall, including the joint between the wall and concrete footing. The repaired wall was tested to failure in the same manner as the original wall. The results showed that the strength and displacement capacities of the wall were completely restored and even exceeded the original capacities.

Marshall and Sweeney (2002) studied the in-plane shear performance of masonry walls strengthened with FRP. In this study a variety of FRP configurations were evaluated. In all cases the FRP was applied to one side of the wall only because, in a typical rehabilitation project, access may not always be feasible to both sides of walls. FRP configurations included both full coverage of the pier section and partial coverage. Depending upon the climate where the FRP would be installed, full coverage could seal up a wall so tightly that the moisture barrier and moisture permeation through the wall is compromised. This could in turn require HVAC modifications to maintain a healthy interior environment. Partial coverage consisted of 20 cm (8 in.) wide strips of FRP placed to strengthen the masonry wall or to modify its failure mode. Figure (2.3) illustrates the different FRP configurations

evaluated. The conclusion reached was that FRP strengthening increased the strength of the wall; however, the failure mode in all cases changed to be less ductile, which does not agree with most of the other studies.

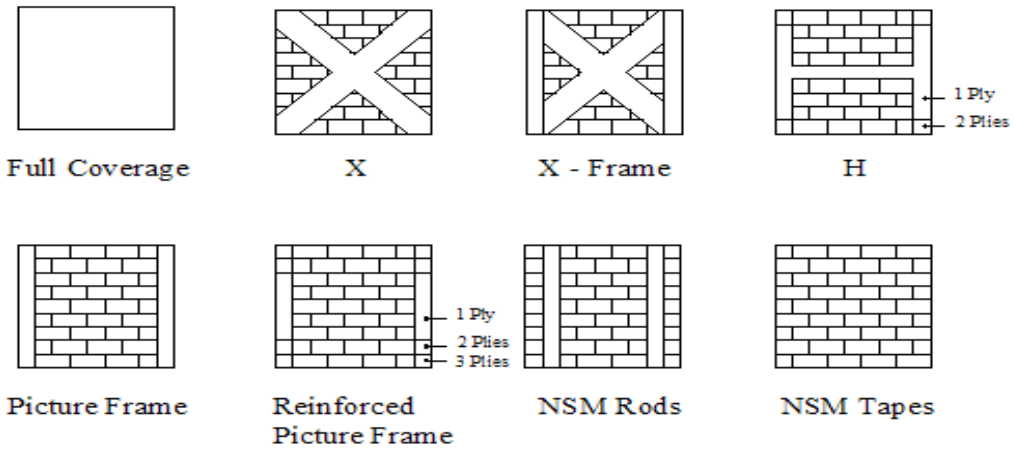

Figure (2.3) FRP reinforcement configurations

Vandergrifi et al. studied the CFRP seismic retrofit of unreinforced masonry walls. In this study, six 1219 mm by 2438 mm masonry walls were tested before and after composite retrofit. Three of the walls (shear specimens) were loaded with in-plane shear forces, and three of the walls (bending specimens) were subjected to out-of-plane bending. Both of these wall types were retrofitted with three different composite laminates.

The retrofitted shear specimens reached a maximum lateral load of 41.6 kN, a strength increase of 1100%. All of these specimens lost their load carrying capacity due to extensive damage near the supports, well before the composite material reached its ultimate strength. The bending specimens reached a maximum of 179.6 kN, which represented an increase of 3100% over the baseline specimens. These bending specimens behaved like traditional composite sandwich panels, which take

advantage of the high tensile/compressive strength material at the face of the inner (masonry) core. The experimental results showed that the FRP laminates significantly increased the in-plane shear and out-of-plane bending capacity of pre-cracked unreinforced hollow masonry walls. Since both wall faces were retrofitted with multiple composite layers, the stress level in the FRP material was well below its ultimate values, clearly indicating that for these tests the masonry governed the results. In Figure (2.4), the in-plane shear specimen at failure is shown and in Figure (2.5) the retrofitted shear specimen at failure is shown.

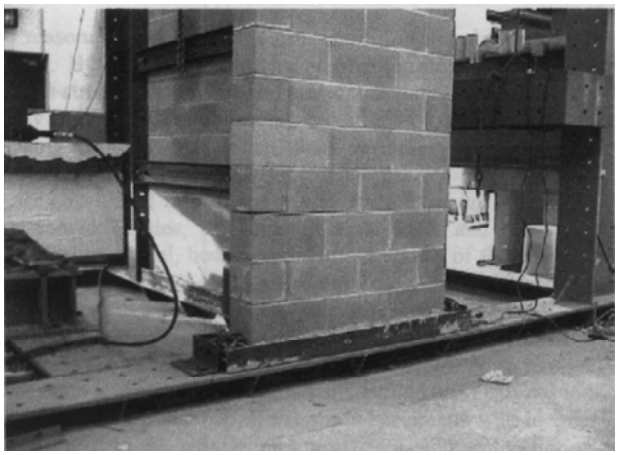

Figure (2.4) In-plane shear specimen at failure

Figure (2.5) Retrofitted shear specimen at failure

2.2.3 Earthquake Simulated Loading

Ghanem et al. (1994) studied the effect of strengthening masonry walls using fiber glass mats (laminates) as external reinforcement to sustain lateral loads induced by an earthquake. The study included testing of 1/3 scale square panels subjected to load diagonal, parallel, and perpendicular to the bed joints. The conclusion reached in that study was that external fiber glass mat reinforcement is an effective strengthening and retrofitting technique, and it has a great potential in improving the strength and deformation properties of hollow concrete masonry.

Ehsani and Saadatmanesh (1996) studied the seismic retrofit of unreinforced masonry wall with fiber composites. Tests were made on both laboratory tested specimens and field specimens to find out the effect of fiber composite retrofitting when loaded both in-plane and out-of-plane.

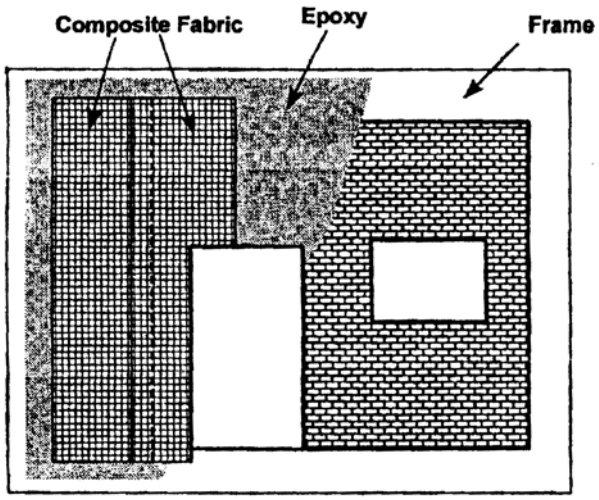

Figure (2.6) Schematic of the proposed strengthening system

Test results indicated that retrofitting of unreinforced masonry structures with composite fabrics is a very effective technique for increasing the flexural and shear strength and ductility of these elements. As for the field specimens (severely damaged buildings during the Northridge earthquake), on which the composites were used, it

proved to be an easy and economical alternative for seismic retrofitting of unreinforced masonry walls. Shown below is the strengthening system [Figure 2.6] proposed by Ehsani and Saadatmanesh, the mechanism for resisting flexure [Figure 2.7], and the mechanism for resisting shear [Figure 2.8].

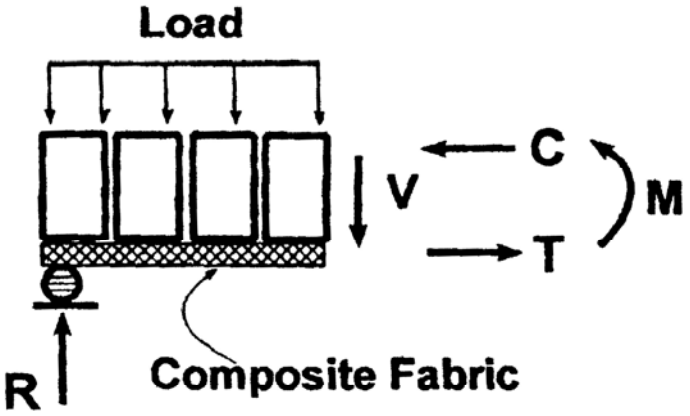

Figure (2.7) Mechanism of resisting flexure

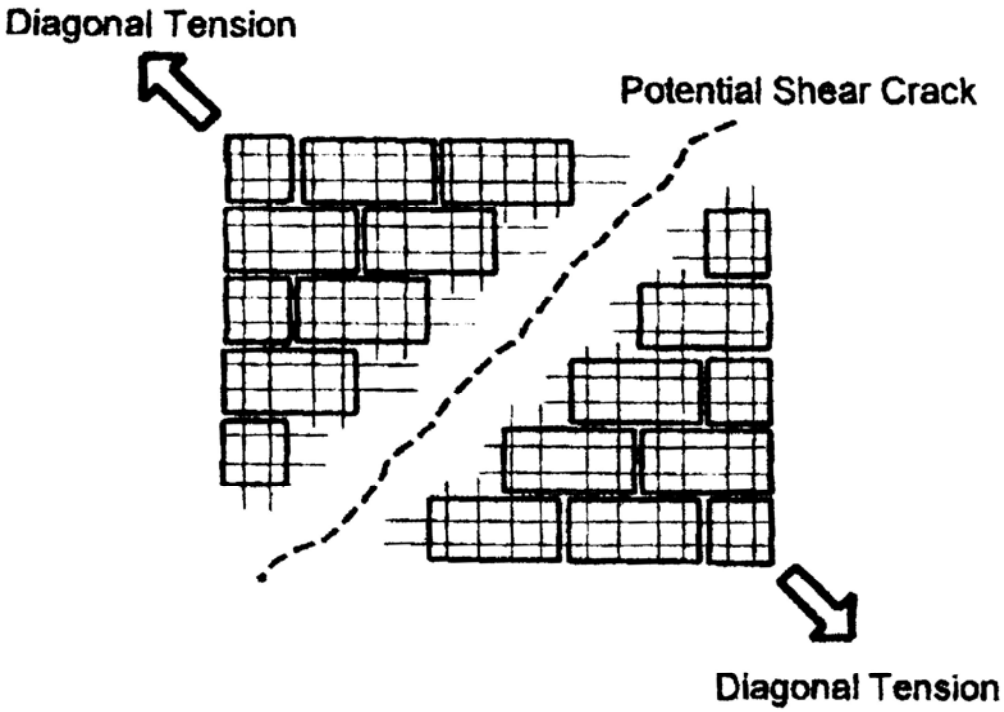

Figure (2.8) Mechanism of resisting shear

Elgwady et al. (2002) studied the dynamic in-plane behavior of unreinforced masonry wall upgraded with composites. In this study, half-scale masonry walls were subjected to a series of simulated earthquake motions on an earthquake simulator, and reached a conclusion that:

- Wall rocking can be a stable nonlinear behavior in URM walls when no out of plane response occurs.
- The lateral resistance of the upgraded specimen was enhanced by a factor of about two compared to the non-upgraded case.

Badoux et al. (2002) compared the effect of earthquake on un-reinforced masonry walls before and after upgrading with composites, using an earthquake simulator. In this study, three half-scale URM test walls were subjected to a series of simulated earthquake motions on an earthquake simulator. The first wall was a reference specimen without upgrading, the following two were upgraded with glass fiber wrap and carbon fiber laminates. The tests lead to the following findings:

- Wall rocking can be a stable nonlinear response in slender un-reinforced masonry walls, providing significant lateral deformation capacity.
- In spite of relatively poor mortar, the wall friction coefficient exceeded 0.55. The wall shear resistance was found to be higher than indicated in available literature.
- The one-sided glass fiber wrap upgrade is promising; it improved the wall lateral resistance by a factor of about two. It also tripled the acceleration corresponding to the onset of nonlinear behavior, thus providing a significant improvement from a “continued operation” limit state point of view.

Nanni and Tumialan (2003) studied the effect of Fiber-Reinforced Composites for the Strengthening of Masonry Structures. In this study, not only the FRP

laminates technique was studied, but also another technique which is called structural re-pointing and consists of near surface mounted fiber reinforced polymer bars. In this technique the FRP bars are placed into a groove cut on the masonry surface as shown in Figure (2.9). The groove is partially filled with an epoxy- or cement-based paste, and the bar is then placed into the groove and lightly pressed to force the paste to flow around the bar. Finally, the groove is filled with more paste and the surface is leveled. This strengthening method does not require sand-blasting and puttying. If hollow masonry units are the base material, special care must be taken to avoid a groove depth exceeding the thickness of the masonry unit shell, and possible local fracture of the masonry. In addition, if an epoxy-based paste is used, strips of masking tape or other similar protection can be attached along the edges of the groove to avoid staining.

The technique named FRP structural re-pointing is a variation of the near surface mounted technique, and consists of placing FRP bars in mortar bed joints. Re-pointing is a traditional retrofitting technique commonly used in the masonry industry for replacing missing mortar in the bed joints. The term “structural” is added because the proposed method allows for restoring the integrity and/or upgrading the shear and/or flexural capacity of a wall. In FRP structural re-pointing, the aesthetics of masonry can be fully preserved. The diameter or width of the FRP bars is limited by the thickness of the mortar bed joint, which usually is not larger than 10mm. Grinding of the mortar bed joints is a simpler task than grooving the masonry units and the spacing of FRP bars is practically dictated by the height of the masonry unit. Here it was found out that by FRP structural re-pointing, the shear capacity and the ductility of unreinforced masonry walls are increased.

Figure (2.9) Encapsulation of fiber reinforced polymer bar

Shrive (2004) studied the use of FRP to improve seismic resistance of masonry walls, columns and arches. He reached a conclusion that there is great potential for the use of FRP to strengthen and rehabilitate masonry with respect to seismic loading. The materials are light weight and very strong. However, strength may not be of great importance as the toughness of the material is, since seismic excitation can induce both in-plane and out-of-plane loading. Moreover, he found out that cracks propagate rapidly and easily between fibers in unidirectional laminates leading to potentially brittle failures, hence, a layer of a material such as sprayed short-fiber GFRP might be more capable of not cracking and not permitting collapse of the masonry.

Bieker et al studied the post-strengthening of masonry columns by use of fiber-reinforced polymers (FRP). Within the scope of that study, test results of post-strengthened masonry columns were presented. Two different types of bricks and two different types of mortars were used to produce the test specimens: vertical coring bricks and solid bricks, calcium cement and calcium mortar. The test specimens were wrapped with two types of fabrics: unidirectional carbon and unidirectional glass tapes with varying numbers of layers. In all cases a thixotropic epoxy system was

used as matrix. The study showed the results of the load bearing behavior of the masonry columns. It was concluded that post-strengthening of masonry columns leads to an essential increase of ultimate load and ductility and for vertical coring bricks an increase of 30 % - 60 % can be achieved depending on the stiffness of the reinforcement.

2.3 Theoretical Analysis of Masonry Walls under In-Plane Loading

Sayed and Shrive (1996) developed a nonlinear elasto-plastic finite-element (FE) model for face-shell-bedded hollow masonry using isoparametric shell elements. The nonlinear behavior of the masonry in compression due to progressive cracking, and geometric and material nonlinearities was considered in the model. Details of the elasto-plastic constitutive model and failure criteria for both blocks and mortar joints were presented. Results from a simulated test of a three-block-high prism were given in the form of stress, strain, and displacement plots. The behavior of the model was compared to known experimental behavior. The modeled specimens gave lower loads than those obtained experimentally because the full extent of mortar crushing and the final buckling out of the face-shells was not modeled.

Zhuge et al. (1998) developed a comprehensive analytical model studying the response of un-reinforced masonry to in-plane dynamic loads, including earthquake loads. The analysis was implemented in a nonlinear finite element program. Masonry was treated as a nonlinear homogeneous orthotropic material. A failure envelope was also developed that was capable of predicting both joint sliding and the cracking and/or crushing types of failure. The effect of bed joint orientation was considered; this was achieved through a ubiquitous joint model. The model is capable of performing both static and time history analyses of masonry structures. Nonlinear

dynamic analysis was carried out using the Modified Newton-Raphson iteration scheme in conjunction with the Newmark time integration algorithm. To calibrate the model and to demonstrate its applications, several numerical examples were treated, and the results were compared with those from full-scale tests on masonry shear walls under both cyclic and dynamic loads.

The conclusion was that the nonlinear behavior of brick masonry is caused by two major effects: progressive local failure (cracking of the mortar) and nonlinear deformation characteristics (in the biaxial compression-compression and uniaxial compression stress state). All these effects were considered in the orthotropic constitutive relations developed in this research. A failure envelope was developed that was capable of predicting both joint sliding and the cracking and/or crushing types of failure for a homogeneous material model. The effect of bed joint orientation was considered. A simple secant-type unloading/reloading curve was adopted for masonry under tension, and the unloading parameter was determined through calibrating the finite element model against experimental results.

The analytical model was validated by comparing results with various experimental results, and reasonably good agreement was found. However, further research could improve the model.

Liu and Dawe (2003) developed and encoded for computer application an analytical technique to study the behavior of concrete masonry load-bearing walls under various loading conditions. Both geometrical and material nonlinearities to account for the moment magnification effect and the degradation of material stiffness were included in the development. Effects of vertical reinforcing steel, masonry tensile cracking, and compressive crushing are included directly in the moment-curvature relationship, which was used in the determination of element stiffness at

successive load increments. A parametric study was conducted following verification of the analytical model by comparing results with experimental test data. Effective flexural rigidity values at failure were obtained analytically and compared with values suggested in the Canadian masonry code CSA-S304.l-M94. It was concluded that CSA-S304l-M94 tends to underestimate effective flexural rigidity values for reinforced walls and thus leads to a conservative design over a range of parameters. Based on approximately 500 computer model tests, a lower bound bilinear limit for the effective rigidity of reinforced masonry walls was established. This limit is believed to provide an accurate and realistic estimate of effective flexural rigidity.

2.4 Basis for Current Study - Experimental Tests on Concrete Masonry Walls

The numerical analysis presented here is based on the experimental study conducted by Allam (2002) and entitled ".In-Plane Cyclic Behavior of Concrete Masonry Walls Enhanced by Advanced Composite Laminates".

Cyclic in-plane shear tests were conducted on six full-scale walls built from reinforced concrete masonry units and strengthened by unidirectional composite laminates. Carbon/epoxy, E-glass/epoxy and pre-cured carbon/epoxy strips were placed on one or both sides of the walls. Each wall sample was loaded with a constant axial load simulating the gravity load, and incremental cyclic lateral shear loads were applied in accordance with the Acceptance Criteria (AC-125) of the International Code Council Evaluation Services (ICC-ES 2003). Displacements, strains and loads were continuously monitored and recorded during all tests. Test results indicated that the limit-state parameter influencing strength gain of the FRP retrofitted walls was the weak compressive strength of the masonry units, especially at the wall toe where high compression stresses exist. Despite such a premature

failure caused by localized compression damage of the masonry at the wall toe, notable improvement in their behavior was achieved by applying the FRP laminates to either one or two sides of the walls. However, it should be cautioned that available theoretical models may significantly overestimate the shear enhancement in the FRP strengthened walls, if other limiting failure modes are not considered. A brief description of the test samples and test results are included here for completeness.

2.4.1 Wall Samples and Material Properties

Six full-scale wall samples were tested under a combination of constant axial load with incremental lateral (push-pull) cyclic loads. As shown in Figure (2.10) and (2,11), each wall specimen was 72 in. (183 mm) high and 72 in. (183 mm) long, and constructed from one wythe of 6 in. x 8 in. x 16 in. (152 mm x 203 mm x 406 mm) hollow concrete blocks. Each wall has a base footing and a top loading reinforced concrete beam. The walls were fully grouted and detailed with five vertical reinforcing bars placed uniformly in the wall. These bars were continuous from the footing base to the top beam without any lap splice, and were strain gauged at the base-wall intersection level to capture the first yield of the steel bars. All wall specimens had a vertical steel reinforcement ratio of 0.54% with no horizontal reinforcement in the direction of the applied shear force to simulate a deficient and/or old wall construction. Four short dowels were distributed between the vertical steel bars at each interface between the wall and both the top loading beam and the footing.

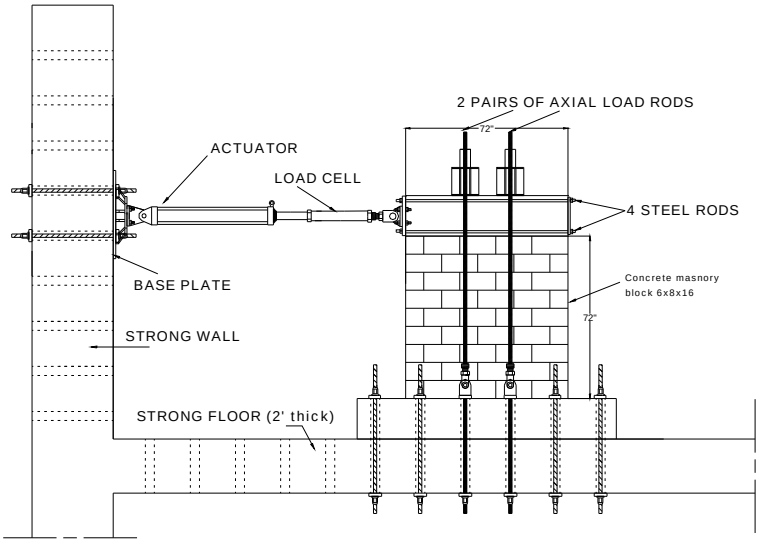

Figure (2.10) Test set-up

Figure (2.11) Gravity and cyclic shear loading on typical wall

As noted above, the wall specimens were built with a height-to-length aspect ratio of 1:1 to promote a shear dominated behavior under in-plane loading. All wall samples were built at the same time, and shared materials from the same batch. The reinforcing bars were grade 60 and were tested, according to ASTM standards, to measure the tensile strength as displayed in Table (2.1).

Table (2.1) Properties of Reinforcing Steel

Bar size	Yield Stress, ksi (MPa)	Ultimate Strength, ksi (MPa)
# 6	60 (414)	94 (648)

Strength tests at 28 days on masonry prisms, grout cylinders, and mortar cylinders yielded 485 psi (3.34 MPa), 2750 psi (18.96 MPa), and 2120 psi (14.62 MPa), respectively. For the carbon/epoxy and E-glass/epoxy laminates, a specimen from each batch, 12 in. x 12 in. (304 mm x 304 mm), was fabricated and tested to ensure the same quality for all retrofitted specimens. All such specimens were tested to obtain their ultimate strength, modulus at yield and strain at ultimate strength as listed in Table (2.2).

Table (2.2) Properties of FRP Composite Materials

Type	Thickness (t) inch (mm)	Ultimate Strength ksi (MPa)	Strain at Ultimate (μ strain)	Modulus of Elasticity ksi (GPa)
Carbon/epoxy	0.045 (1.14)	154 (1,061)	0.012	$14x10^3$ (96.5)
E-glass/epoxy	0.045 (1.14)	74 (510)	0.022	$3.5x10^3$ (24.2)
Carbon strips	0.047 (1.19)	420 (2,896)	0.018	$22x10^3$ (151.7)

2.4.2 General Test Observations

The control as-built wall was cyclically tested to failure and demonstrated a pure shear mode. The failure of the specimen was initiated by diagonal shear cracks and developed a diagonal strut action resulting in the crushing of the wall edge boundaries under compressive stresses.

The predominant mode of failure in all single-side strengthened wall specimens was in the form of shear failure of the un-strengthened side of the wall. This shear failure was a combination of diagonal tension cracks as well as step cracks initiated at the base of the un-strengthened face. However, unlike the as-built specimen, single-side strengthened wall specimens suffered from another mode of localized failure in the form of a compression crushing of one of the wall toes. In fact, this localized failure mode at the wall toes was the controlling factor in determining the ultimate capacity of the single-side strengthened wall specimens.

The common mode of failure of all two-side FRP strengthened wall specimens was also compressive failure of the masonry units at the bottom ends (toes) of the wall specimens. The application of the composite laminates to the two sides of the wall specimens contributed an appreciable stiffness gain which was evident from the displacement profiles of such specimens. However, the overall usable strength gain was limited by the masonry compression properties rather than the ultimate tensile strength of the unidirectional FRP laminates. This applies to all FRP strengthening systems evaluated in this study, including E-glass/epoxy wet lay-up laminates, carbon/epoxy wet lay-up laminates, and pre-cured unidirectional carbon/epoxy strips. The premature compression failure of the wall toes resulted in appreciable shear and flexural stiffness degradations that was amplified by the loss of the grout confinement leading to local buckling of the vertical steel bars near the ends of the walls. Table (2.3) presents a summary of the ultimate strength of the tested specimens.

Table (2.3) Ultimate Strength of Tested Wall Samples

Description	Ultimate Strength, kips (kN)
Control (ultimate)	83 (369.18)
Carbon/epoxy repair (two sides)	100 (444.8)
Carbon/epoxy retrofit (single side)	95 (422.6)
Carbon/epoxy retrofit (two sides)	108 (480.38)
E-glass/epoxy retrofit (two sides)	106 (471.49)
Carbon strips retrofit	98 (435.9)

CHAPTER 3

DESIGN FORMULAE AND ENGINEERING SOLUTIONS

3.1 Design Formulae for Lateral Capacity of Masonry Walls

The in-plane shear capacity of masonry walls, denoted by V, may be expressed as the sum of two main components: the shear strength of the masonry, denoted by V_m, and the shear strength of the retrofitting FRP system which is denoted by V_s. Therefore,

$$V = V_m + V_s \tag{3.1}$$

3.1.1 Shear Strength of Masonry

Due to Drysdale et al (1999), the shear strength of the masonry can be estimated using the following equation

$$V_m = v_m d_w t_w \tag{3.2}$$

where

$$d_w = 0.8 L_w \tag{3.3}$$

and

$$v_m = 2.0\sqrt{f'_m} + 0.3(P_{ax} / A_g) \le 110 + 0.3(P_{ax} / A_g) \le 190 \text{ psi} \tag{3.4a}$$

and for SI units

$$v_m = 0.17\sqrt{f'_m} + 0.3(P_{ax} / A_g) \le 0.75 + 0.3(P_{ax} / A_g) \le 1.3 \text{ MPa} \tag{3.4b}$$

where d_w is the effective length of the wall, L_w is the actual length of the wall, t_w is the wall thickness, f'_m is the masonry crushing strength, P_{ax} is the axial load on the wall, A_g is the gross cross sectional area and v_m is the masonry shear stress.

According to Equation (3.2), the shear strength contributed by the masonry V_m is calculated as 41.14 kips (183.1 kN).

3.1.2 Shear Strength of FRP Laminates

The shear strength of carbon and E-glass laminates is calculated according to the ICC-ES Acceptance criteria (AC125) for Concrete Reinforced Masonry Strengthening Using Fiber-reinforced Polymer (FRP) Composite System.

According to section 7.3.2.6.3 of the AC125 document, the shear strength enhancement for rectangular wall sections of length, *H,* in the direction of the applied shear force, with a laminate thickness, t_f, on two sides and one side of the wall at an angle, θ, to the wall axis is calculated by the following equations

A) Two-sided

$$V_s = 2t_f f_j H \sin^2 \theta \tag{3.5}$$

B) Single-sided

$$V_s = 0.75t_f f_j H \sin^2 \theta \tag{3.6}$$

where

$$f_j = 0.004\, E_j \leq 0.75\, f_{uj} \tag{3.7}$$

in which f_j is the hoop stress developed in the jacket material, psi; E_j is the longitudinal modulus of elasticity of the FRP composite material, psi; and f_{uj} is the ultimate tensile strength of the composites, psi.

Therefore, using the properties of the masonry and the FRP laminates as identified at the end of Chapter (2), one can estimate the expected lateral capacities of the tested wall samples of the experimental program reported by Allam (2002). These capacities are highlighted in Table (3.1) for the tested samples and are also presented for other configurations as well.

Table (3.1) Lateral Capacities of Walls Retrofitted by FRP Laminates

Wall Specimen	Calculated Strength of Laminates (kips)	Total Capacity of Retrofitted Wall (kips)
1 Carbon laminate on 1 side only	136	177 (95)*
1 Carbon laminate on each side	363	404 (108)*
2 Carbon laminates on 1 side only	272	313
2 Carbon laminates on each side	726	767
1 Glass laminate on 1 side only	34	75
1 Glass laminate on each side	91	132
2 Glass laminates on 1 side only	68	109
2 Glass laminates on each side	182	223 (106)*

* Experimental Results

3.2 Engineering Solutions

The experimental program showed that the failure mode of the retrofitted samples was more or less due to the crushing of masonry blocks under global flexure of the wall rather than due to in-plane shear for the unretrofitted wall sample. Therefore, one can approximately estimate the ultimate capacity of the wall by computing the lateral force that may cause crushing of the masonry blocks at the wall's toe.

3.2.1 Wall Capacity Based Only on Equilibrium

The flexural capacity of the wall specimen can be determined assuming an under-reinforced condition for the section and neglecting steel on the compression side. The depth of the stress block, a, assuming rectangular stress block, is

$$a = \frac{A_s f_y + P_s + P_w}{0.85 f_m^{'} b_e} \tag{3.8}$$

where b_e is the effective thickness of masonry at the critical section, A_s is the cross-sectional area of the reinforcing steel, f_y is steel yield strength, and $f^{'}_m$ is the masonry compressive strength.

Applying the moment equation for the set of forces acting on the wall specimen gives

$$M_{n,bar} = A_s f_y (d - a/2) + (P_s + P_w)(l/2 - a/2) \tag{3.9}$$

where $M_{n,bar}$ is the moment capacity acting on the wall section, d is the depth from the wall end to the far most rebar on the tension side, P_s is the axial load applied on the top of the wall, P_w is the weight of the wall specimen, and l is the length of the wall.

Based on Equations (3.8) and (3.9), the depth of the stress block is 9.3 inch (236 mm) and the moment capacity is 5,134 kips.in (580 kN.m). Dividing the moment capacity by the wall height, the flexural capacity is about 71.5 kips (318 kN). This calculated capacity of the wall is less than the actual capacity, which shows that the used approach is conservative.

3.2.2. Wall Capacity Based on Equilibrium and Strain Compatibility

The flexural strength of the wall is estimated by dividing the moment capacity of the wall section corresponding to the first yield by the height of the specimen as recommended by Pauley (1992). Figure (3.1) shows the first yield flexural condition of the wall. Under the assumption of a linear strain, the flexural strength M_i can be calculated by Equation (3.10). The neutral axis c is determined to satisfy Equation (3.11). An ultimate crushing strain of 0.002 is considered for the unconfined masonry.

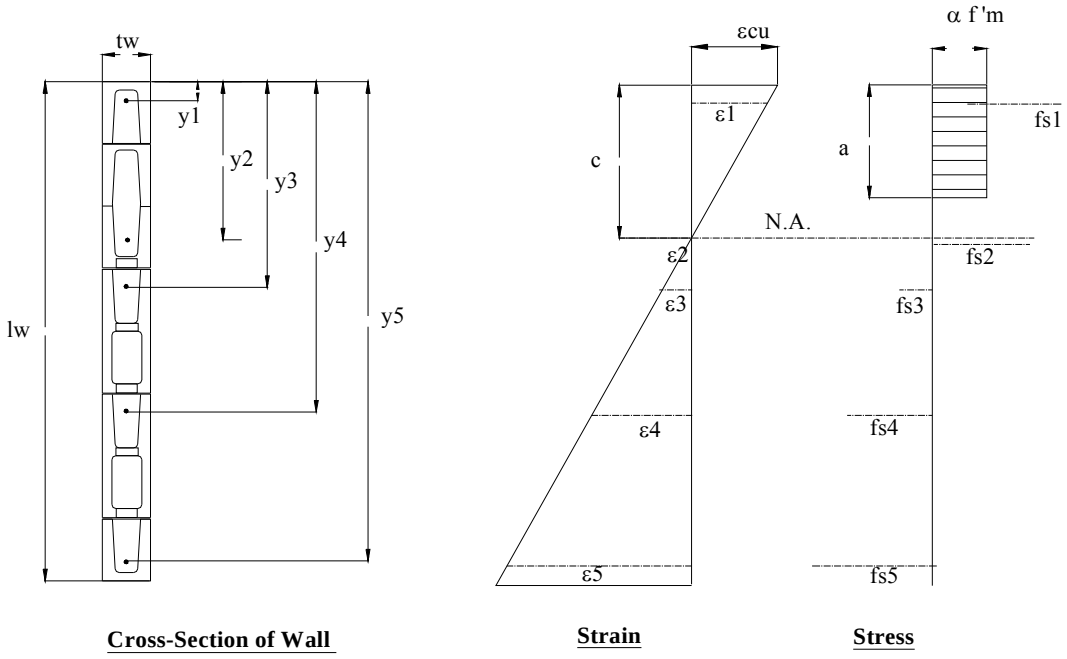

Figure (3.1) First yield flexural condition

$$M_i = C_m\left(\frac{l_w}{2} - \frac{a}{2}\right) + \sum_{i=1}^{n} f_{si} A_{si}\left(\frac{l_w}{2} - y_{si}\right) \tag{3.10}$$

$$C_m + C_s = P_{ax} + T_s \tag{3.11}$$

$$C_m = \alpha\, f_m^{'}\, t_w\, a\,, \qquad a = 0.85\, c \tag{3.12}$$

$$C_s = \sum_{i=1}^{j} A_{si} f_{si}\,, \qquad T_s = \sum_{i=j+1}^{n} A_{si} f_{si} \tag{3.13}$$

where C_m is the masonry compression force, C_s is the steel compression force with bars *1* through *j* in compression, T_s is the steel tension force with bars *j+1* through *n* in tension, P_{ax} is the axial load, *c* is the neutral axis depth, f'_m is the uniaxial masonry compressive strength, *t* is the wall thickness, y_{si}, A_{si}, f_{si} are position, cross sectional area and steel stress, respectively, of the i^{th} reinforcing bar, *n* is the total number of

reinforcing bars and t_w is the wall thickness. Substituting in Equation (3.10), c was calculated to be 18.9 inch (480 mm) and the flexural capacity is 120 kips (534 kN).

The above simple approach confirms that the wall capacity cannot achieve the values recommended in the design formulas which are based only on the strength provided by the FRP laminates and not having taken into consideration the crushing mode of the masonry blocks at the wall's toe.

CHAPTER 4

FINITE ELEMENT MODELING

4.1 Model and Mesh Creation

The finite element model was created using the ABAQUS CAE which is the preprocessor of the ABACUS solver. On ABAQUS CAE the mesh was established and the nodes and elements sets were assigned. The drafted wall model is then exported as a text input file.

On the input file the reinforcing steel is then generated. The materials properties are selected and section properties for the components of the wall are specified.

After all wall mechanical and physical properties were defined, the boundary conditions and the loading conditions on the walls were created, and finally output is requested for the wall.

4.2 Model Description

The wall model is composed of two types of elements. The first type is the layered thick shell element (S4 element) which is used to represent the masonry wall and the FRP laminates, if present. The second type is the truss element (T3D2) which is used to represent the reinforcing steel in the masonry wall.

4.2.1 Shell Elements for Masonry Wall and Composite Laminates

Element type S4 is a fully integrated, general-purpose, finite-membrane-strain shell element available in ABAQUS/Standard. The element's membrane response is

treated with an assumed strain formulation that gives accurate solutions to in-plane bending problems, is not sensitive to element distortion, and avoids locking.

Element type S4 element has four integration locations per element. S4 can be used for problems prone to membrane- or bending-mode hourglassing, in areas where greater solution accuracy is required, or for problems where in-plane bending is expected. S4 cannot be used with the hyperelastic or hyperfoam material definitions.

The element can be defined as a laminated (layered) shell made of one or more materials. Optionally, one can specify an overall orientation definition for the composite section lay-up. In general, for each layer of the shell, one may specify the thickness, the number of integration points (see below), the material type, and the orientation (either as a reference to an orientation definition or as an angle measured relative to the overall orientation definition). The order of the laminated shell layers with respect to the positive direction of the shell normal is defined by the order in which the layers are specified.

4.2.1.1 Shell Layers: For continuum shell elements, the thickness is determined from the element geometry and may vary through the model for a given section definition. Hence, the specified thicknesses are only relative thicknesses for each layer. The actual thickness of a layer is the element thickness times the fraction of the total thickness that is accounted for by each layer. The thickness ratios for the layers need not be given in physical units, nor do the sum of the layer relative thicknesses need to add to one. The specified shell thickness is used to estimate certain section properties, such as hourglass stiffness, which are later computed using the actual thickness established from the element geometry.

An example of a section with three layers and three integration points per layer is shown in Figure (4.1).

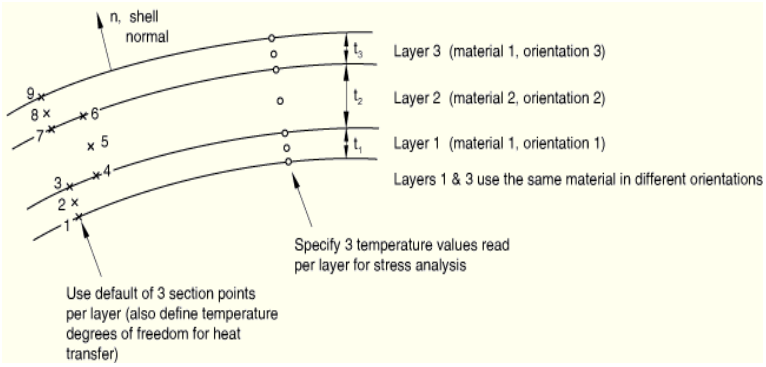

Figure (4.1) Example of composite shell section definition

The material name specified for each layer refers to a material definition. The material behavior can be linear or nonlinear.

The orientation for each layer is specified by either the name of the orientation associated with the layer or the orientation angle in degrees for the layer. This orientation angle (degrees), φ, is measured positive counterclockwise around the normal and relative to the overall section orientation, where $-90^{o} \leq \varphi \leq 90^{o}$. If either of the two local directions from the overall section orientation is not in the surface of the shell, φ is applied after the section orientation has been projected onto the shell surface. If one does not specify an overall section orientation, φ is measured relative to the default local shell directions.

The section properties must be associated with a region of the model.

4.2.1.2 Shell Section Integration: Simpson's rule and Gauss quadrature are available to calculate the cross-sectional behavior of a shell. One may specify the number of integration points through the thickness of each layer for the integration method as described. The default integration method is Simpson's rule with five points for a homogeneous section and Simpson's rule with three points in each layer for a composite section.

The three-point Simpson's rule and the two-point Gauss quadrature are exact for linear problems. The default number of integration points should be sufficient for nonlinear applications (such as predicting the response of an elastic-plastic shell up to limit load). Gaussian integration normally requires no more than five integration points.

Simpson's integration rule should be used if results output on the shell surfaces or transverse shear stress at the interface between two layers of a composite shell is required and must be used for heat transfer and coupled temperature-displacement shell elements.

4.2.2 Truss Elements for Reinforcing Steel

Truss elements are used in two and three dimensions to model slender, line-like structures that support loading only along the axis or the centerline of the element. No moments or forces perpendicular to the centerline are supported.

The two-dimensional truss elements can be used in axisymmetric models to represent components, such as bolts or connectors, where the strain is computed from the change in length in the **r–z** plane only. Two-dimensional trusses can also be used to define master surfaces for contact applications in ABAQUS/Standard. In this case, the direction of the master surface's outward normal is critical for proper detection of contact.

The 3-node truss element available in ABAQUS/Standard is often useful for modeling curved reinforcing cables in structures, such as pre-stressed tendons in reinforced concrete or long slender pipelines used in the off-shore industry.

Truss elements in ABAQUS are named as follows:

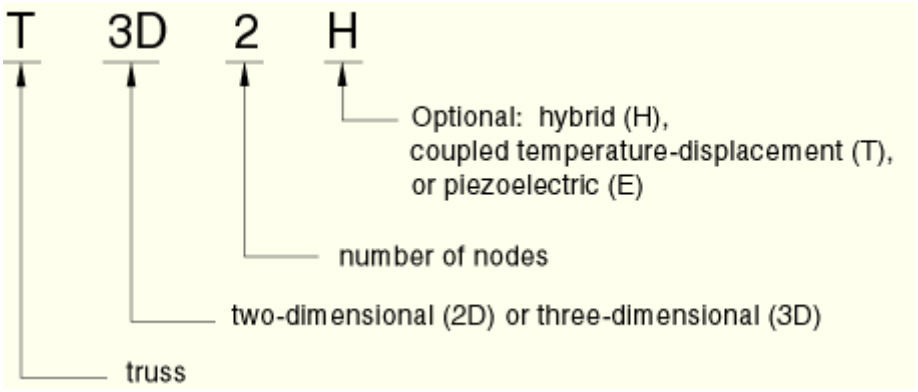

Figure (4.2) Naming of Truss Elements in ABAQUS

4.2.2.1 Element Normal Definition: For two-dimensional trusses the positive outward normal, $\mathbf{n}$, is defined by a 90° counter clockwise rotation from the direction going from node 1 to node 2 or node 3 of the element, as shown in Figure (4.3).

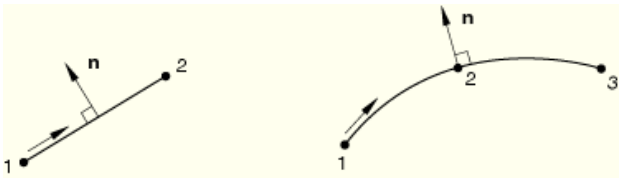

Figure (4.3) Positive outward normal, $\mathbf{n}$, definition by a 90° counter clockwise rotation from the direction going from node 1 to node 2 or node 3 of the element

One can define the cross-sectional area associated with the truss element as part of the section definition. If one does not specify a value for the cross-sectional area, unit area is assumed.

When truss elements are used in large-displacement analysis, the updated cross-sectional area is calculated by assuming that the truss is made of an incompressible material, regardless of the actual material definition. This assumption affects cases only where the strains are large. It is adopted because the most common

applications of trusses at large strains involve yielding metal behavior or rubber elasticity, in which cases the material is effectively incompressible.

4.2.2.2 Large-Displacement Implicit Analysis: Truss elements have no initial stiffness to resist loading perpendicular to their axis. If a stress-free line of trusses is loaded perpendicular to its axis in ABAQUS/Standard, numerical singularities and lack of convergence can result. After the first iteration in a large-displacement implicit analysis, stiffness perpendicular to the initial line of the elements develops, sometimes allowing an analysis to overcome numerical problems.

In some cases loading the truss elements along their axis first or including initial tensile stress can overcome these numerical singularities. However, one must choose the magnitude of the loading or initial stress such that the final solution is unaffected.

4.3 Finite Element Mesh

4.3.1 Uniform Mesh

The analysis of the wall model was initially performed using a uniform mesh size of 4x4; however, two other mesh sizes were examined to reach the optimal mesh size that may yield the expected experimental results. Theoretically, all reasonably small mesh sizes should give the same results for same wall configurations with only minor differences, but here it was found out that the mesh size matters significantly. Because the program computes an average of the stresses in an element, it does not capture the maximum stress especially when the mesh gets bigger in dimensions in the critical zones.

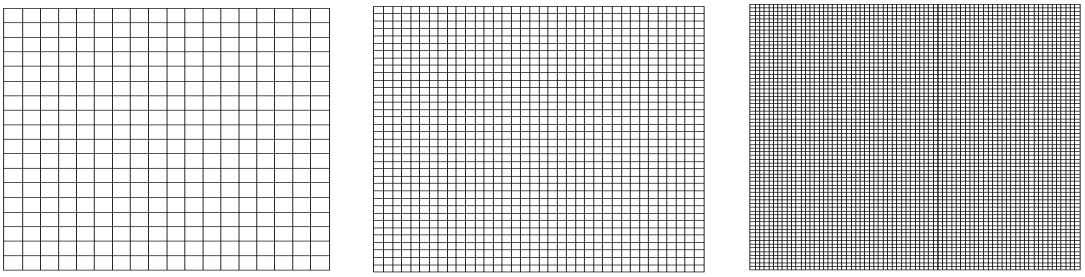

Figure (4.4) Uniform 4x4, 2x2 and 1x1 Mesh, respectively

Figure (4.4) shows the three uniform mesh sizes used in the analysis: 4x4 inch, 2x2 inch, and 1x1 inch. The latter was found to produce results of acceptable accuracy when compared to the experimental results.

4.3.2 Non Uniform Mesh

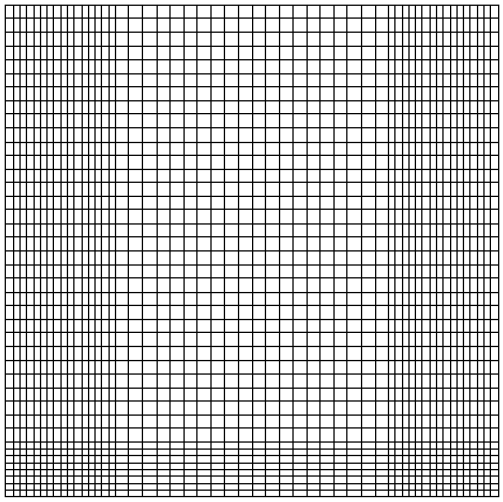

Figure (4.5) Non Uniform Mesh

This mesh was divided into six regions where the lower two corners were meshed to be 1x1. In between the two corners, the mesh size was 2x1. Above the two corners, the mesh size was 1x2 and in the middle of the wall the mesh size was 2x2.

The mesh was selected so that the mesh density is high at the lower corners where failure is expected to take place. This mesh distribution produced much lower

number of elements than the 1x1 mesh all over the wall (less than half the number) and it provided acceptable results.

4.4 Analysis Procedure

The analysis of the masonry wall consists of two steps:

A. Analysis Step-1: The first analysis step includes the application of a constant distributed normal edge load on the masonry top using the ABAQUS command [EDNORn] where n denotes the element edge number upon which the distributed load is applied. The distributed normal edge load value is (108 kips/72 inch = 1.5 kips/ inch).

B. Analysis Step-2: The second analysis step includes the application of the monotonically increasing distributed shear edge load on the top using the ABAQUS command [EDSHRn]. It is important to mention that the loading applied in analysis step-2 is added to the constant loading in analysis step-1. The distributed maximum shear value may reach is (120 kips/72 inch = 1.67 kips/inch) unless the wall fails at a lower value.

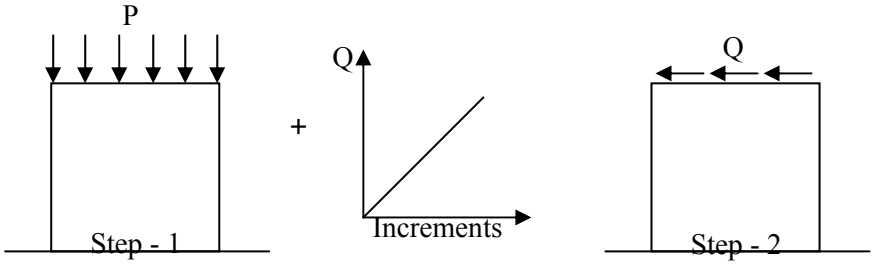

Figure (4.6) Load application

4.5 Boundary Conditions

The walls were fixed in six degrees of freedom at the base and the rest if the wall was fixed in three degrees of freedom which are the displacement in the Z-direction, the rotation about the X- axis and the rotation about the Y-axis.

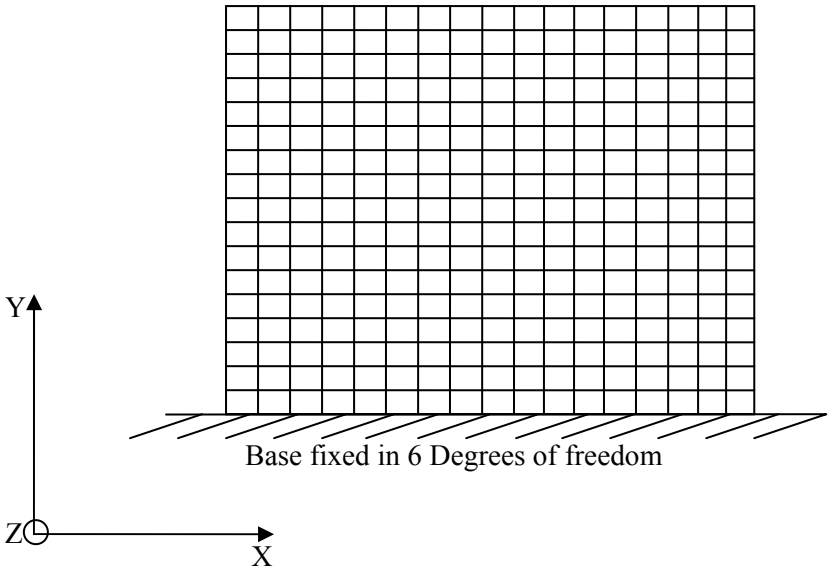

Figure (4.7) Boundary conditions and coordinate axes (X,Y and Z)

4.6 FRP [No Compression] Command

Fiber reinforced laminates are extremely efficient in resisting tension but incapable of resisting compression. The [NO COMPRESSION] option prevents any compressive stresses with in the fiber reinforced laminates. This command is available only in ABAQUS/Standard. Hence all simulations involving laminates must be done using ABAQUS/Standard.

4.7 Illustrative Results

4.7.1 Effect of Mesh Size

4.7.1.1 Wall with No Steel and No Laminate 4 x 4 Mesh: In this specimen the wall failed at Load level of 70 kips with a displacement of 0.14 inch. The stress distribution in the Y- direction is shown in Figure (4.8) and the magnitude of the plastic strain is shown in Figure (4.9) showing the area at which failure took place; this failure pattern was repeated in all specimens.

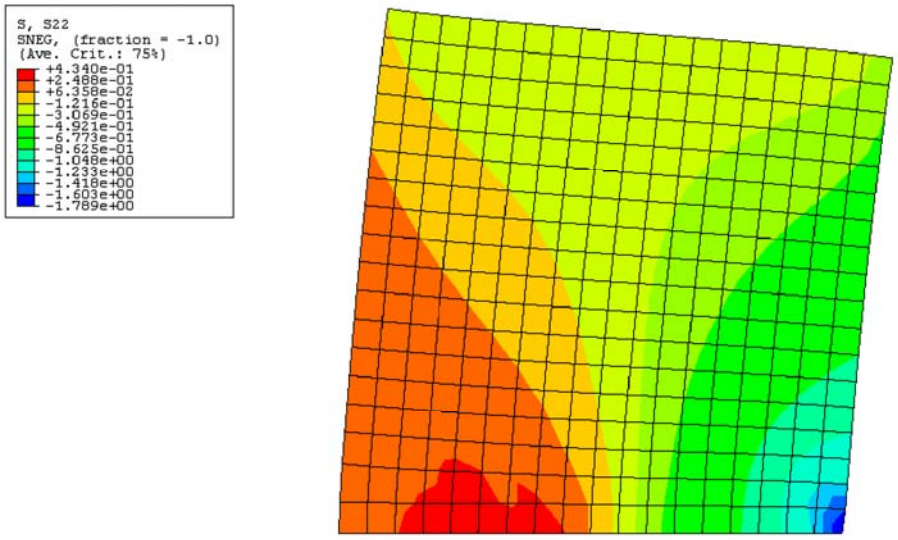

Figure (4.8) Stress distribution in the vertical direction for a wall with no steel and no laminate (4 x 4 mesh)

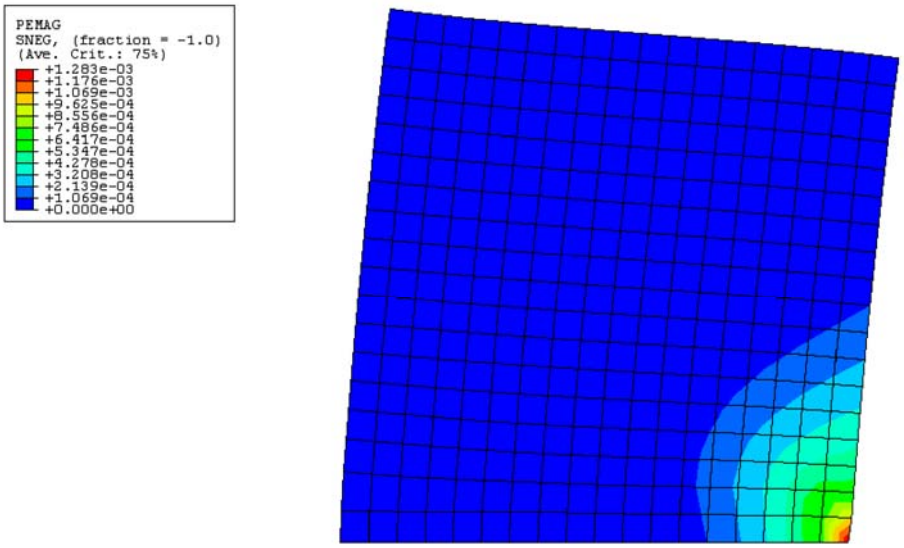

Figure (4.9) Plastic strain for a wall with no steel and no laminate (4 x 4 mesh)

4.7.1.2 Wall with No Steel and No Laminate 2 x 2 Mesh: In this case, the 4x4 mesh was reduced to a 2x2 mesh to attempt obtaining more accurate results and exhibit a real wall that would fail in an experiment. However, the results were still not satisfactory. In this specimen, the wall failed at load level of 65 kips with a displacement of 0.119 inch. The stress distribution in the Y- direction is shown in Figure (4.10)

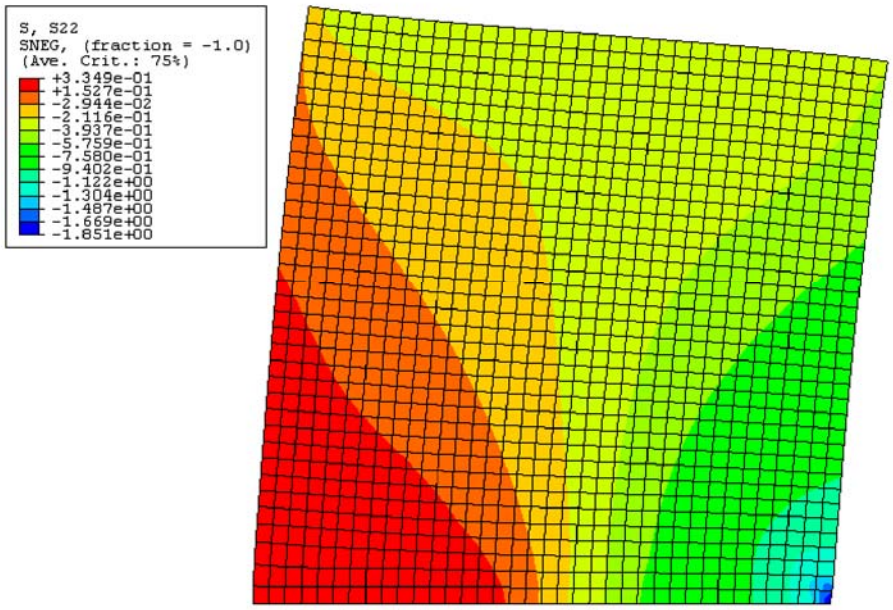

Figure (4.10) Stress distribution in the vertical direction for a wall with no steel and no laminate (2 x 2 mesh)

4.7.1.3 Wall with No Steel and No Laminate 1 x 1 Mesh: In this specimen the mesh was reduced to 1x1 inch. This mesh gave acceptable results which were nearly the same as the results produced by the non uniform mesh. It was decided to work the rest of the specimens using this mesh for accuracy.

In this specimen the wall failed at load level of 55 kips with a displacement of 0.0849 inch. The stress distribution in the Y- direction is shown in Figure (4.11).

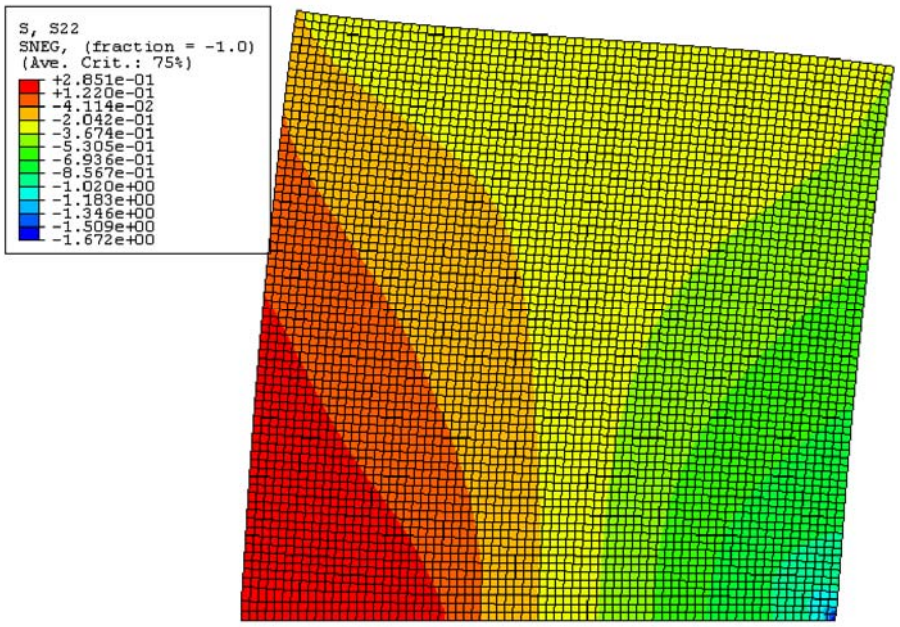

Figure (4.11) Stress distribution in the vertical direction for a wall with no steel and no laminate (1 x 1 mesh)

4.7.1.4 Wall with No Steel and No Laminate Non Uniform Mesh: In this specimen, the wall failed at load level of 55 kips with a displacement of 0.0847 inch. The stress distribution in the Y- direction is shown in Figure (4.12).

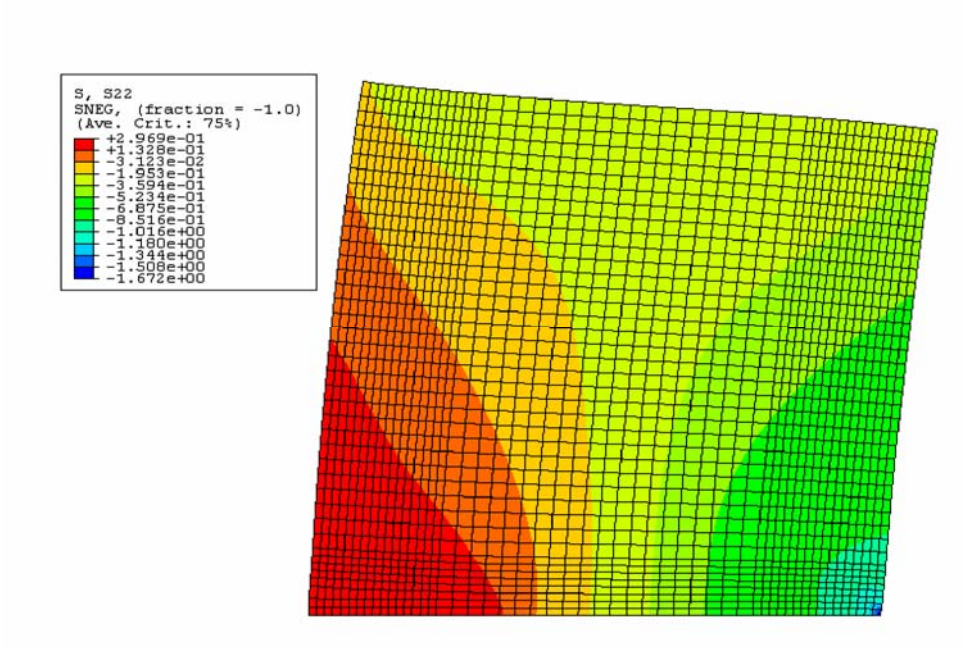

Figure (4.12) Vertical stress distribution (non uniform mesh)

4.7.2 Effect of Steel Reinforcement

4.7.2.1 Sample of Stress Distribution in Reinforcing Truss Element: In all specimens the steel did not reach the yield, meaning that the masonry failed before the steel, yet it increased the failure load of the masonry. Figure (4.13a) shows the stress distribution in the reinforcing steel in the wall after applying the vertical dead load, whereas Figure (4.13b) shows the stress in steel at the end of lateral loading. The failure load of the non retrofitted wall increased from 55 kips to 85 kips.

4.7.3 Effect of FRP Laminates

4.7.3.1 Wall with No Steel and Two Layer Carbon Laminates on Each Side - Non Uniform Mesh: This analysis was performed to find out the effect of carbon laminates on the wall and it was found out that the laminates had a great effect in strengthening the wall; however the wall deflection was relatively high.

In this specimen the wall failed at load level of 100 kips with a displacement of 0.175 inch. The stress distribution in the Y-direction is shown in Figure (4.14) whereas Figure (4.15) shows a sample of the laminate layer having no compression stresses.

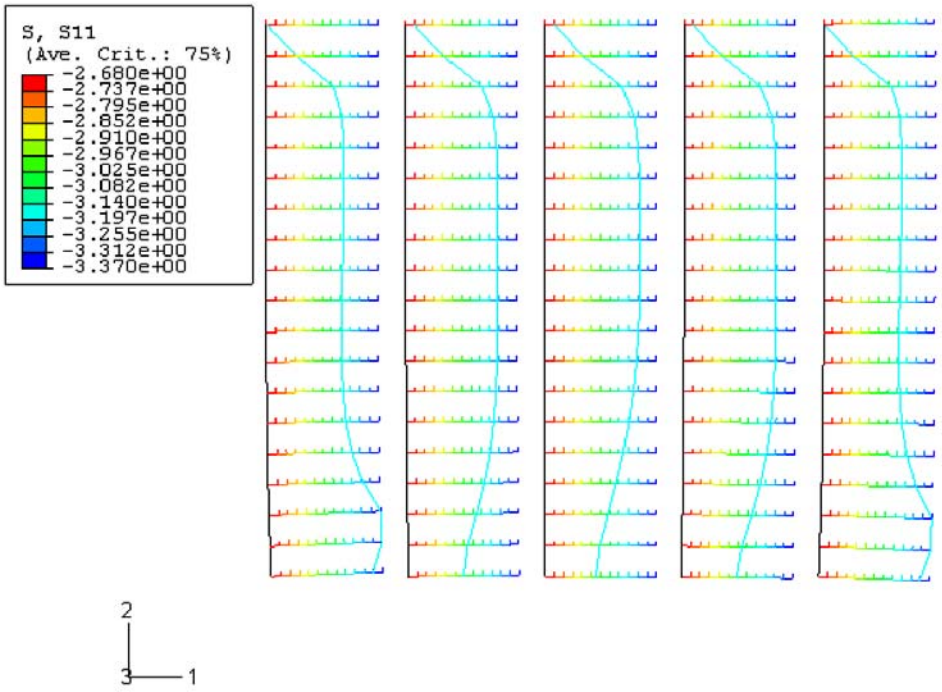

Figure (4.13a) Stress distribution in reinforcing steel after application of vertical load

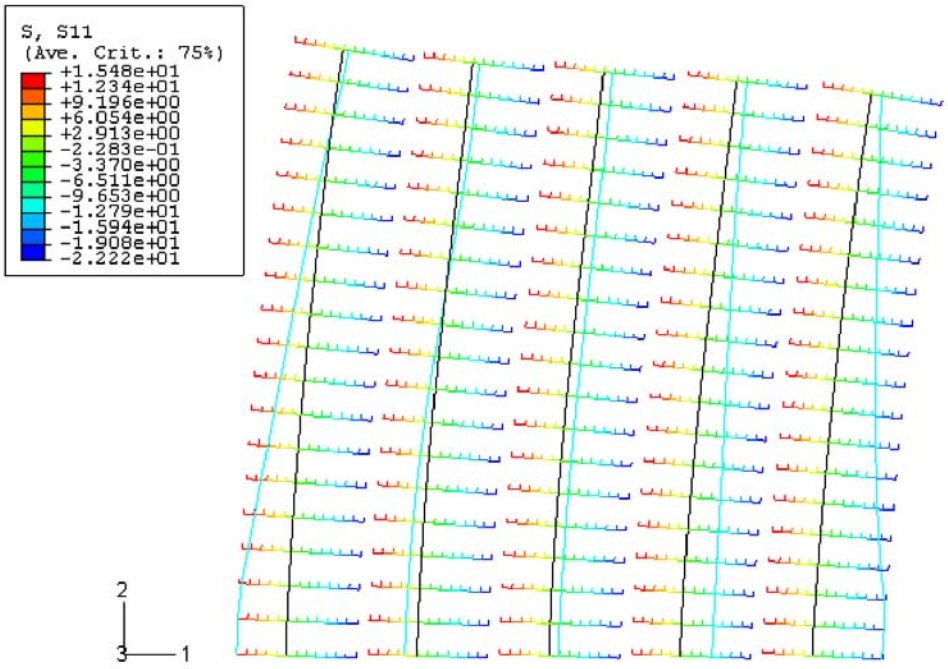

Figure (4.13b) Stress distribution in reinforcing steel after adding the lateral load

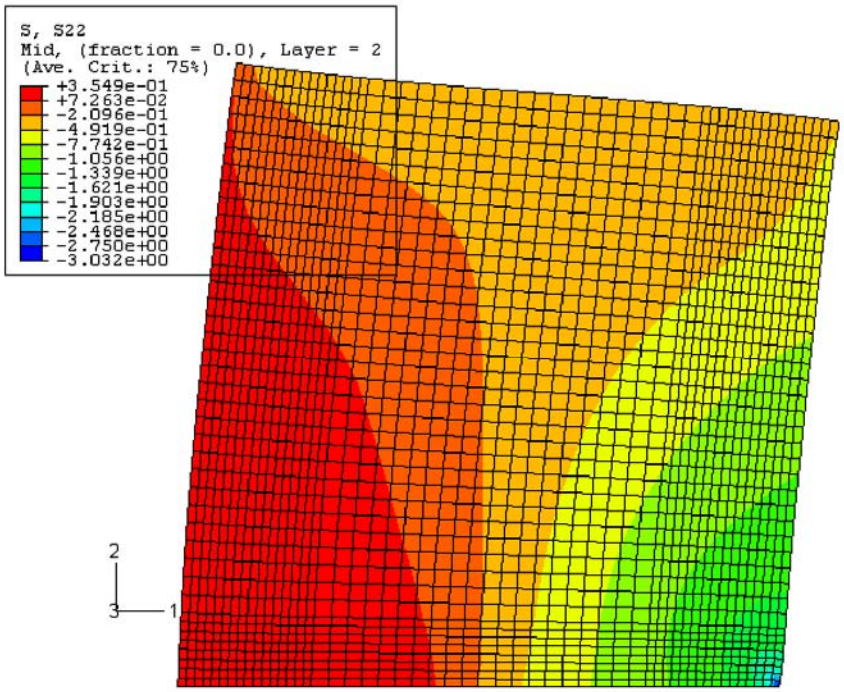

Figure (4.14) Vertical stress distribution in a wall with no steel and two-layer carbon laminates on each side with a non uniform mesh

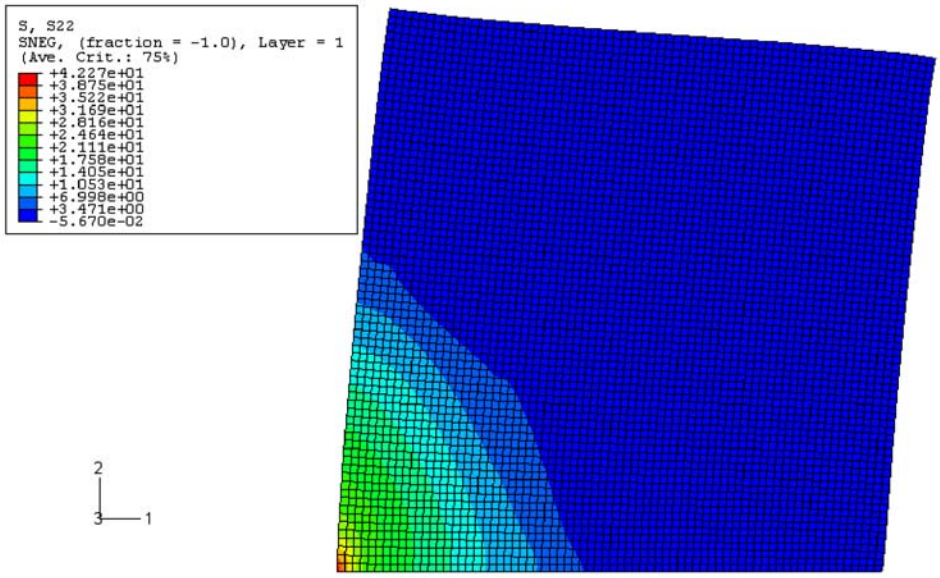

Figure (4.15) FRP carbon laminates with no compression stresses in the Y-direction

4.7.4 Effect of Modulus of Elasticity

4.7.4.1 Wall with Steel and No Laminate 1 x 1 Mesh E=2100 Ksi: In this specimen the modulus of elasticity of the wall was calculated according to the volume of grout, mortar and masonry in the wall; however, this calculated value was very rough and caused the wall to be very rigid so it had to be reduced to get results which are closer to a real wall. In this specimen the wall failed at a load level of 75 kips with a deflection of 0.0615 inch.

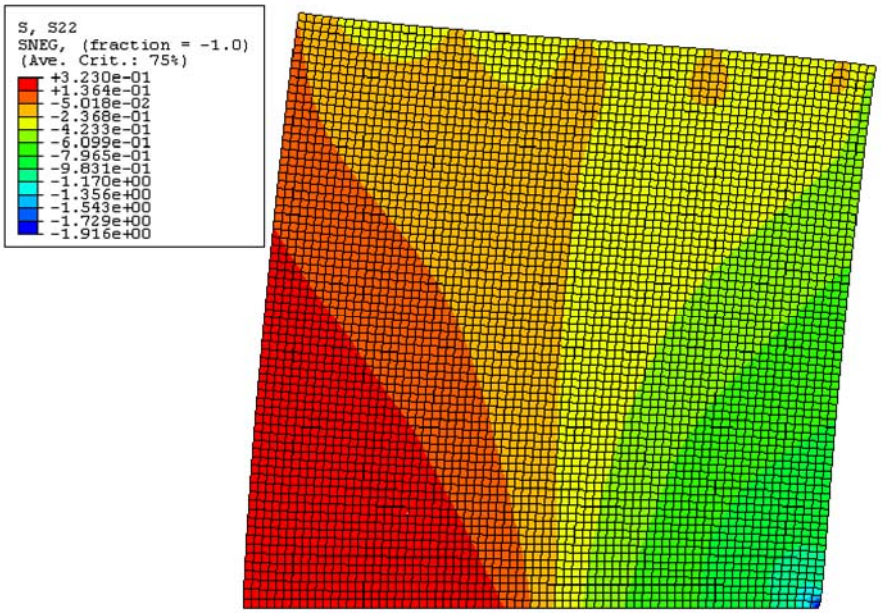

Figure (4.16) Vertical stress in wall with steel and no laminate (E=2100 Ksi)

4.7.4.2 Wall with Steel and No Laminate 1 x 1 Mesh E=950 Ksi: This specimen was performed to examine the effect of the modulus of elasticity; after trials, it was reduced to 950 Ksi. Accordingly, the wall specimen failed at a load level of 85 kips with a deflection of 0.132 inch which is very close to the experimented wall.

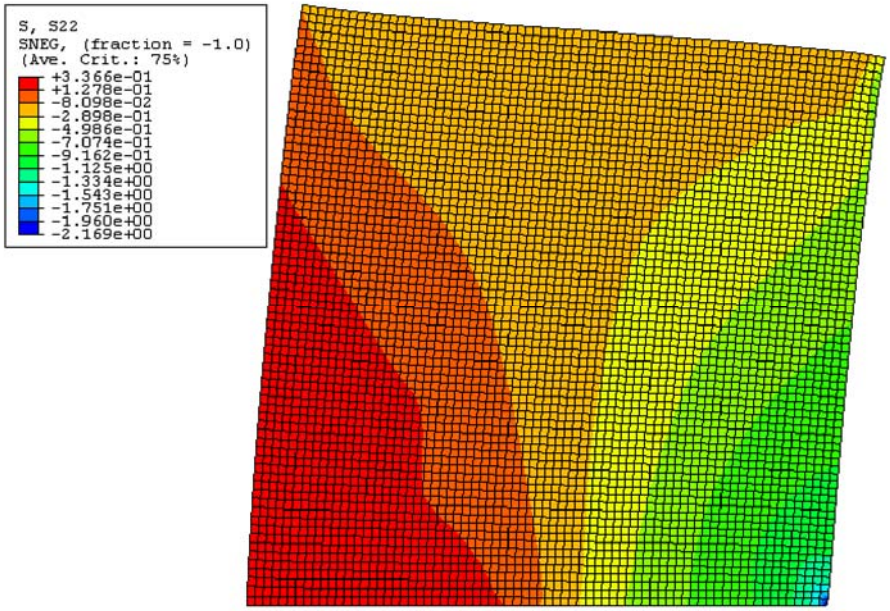

Figure (4.17) Vertical stress in wall with steel and no laminate (E=950 Ksi)

4.7.5 Effect of Restraints

In the common analysis, the wall was restrained in all six degrees of freedom at the base and the rest of the wall was restrained in three degrees of freedom, in the Z- direction and the rotation around the X and Y axes. This essentially forces the wall to deform in its plane of symmetry. The wall that was retrofitted by two laminates from one side as such would be identical to the walls retrofitted by one layer on each side of the wall. In the essence, this eliminates the expected reduction in strength due to asymmetry.

Accordingly two specimens were examined to see the effect of the boundary conditions on the wall. In these two specimens the wall was fixed at the base and the rest of the wall was not restrained.

4.7.5.1 Wall Fixed at Base Only: In this specimen the wall failed at a load of 85 kips, which is the same failure load of a wall that was restrained in six degrees of

freedom at the bottom and the rest of the wall restrained in the Z direction and the rotation around the X and Y axes.

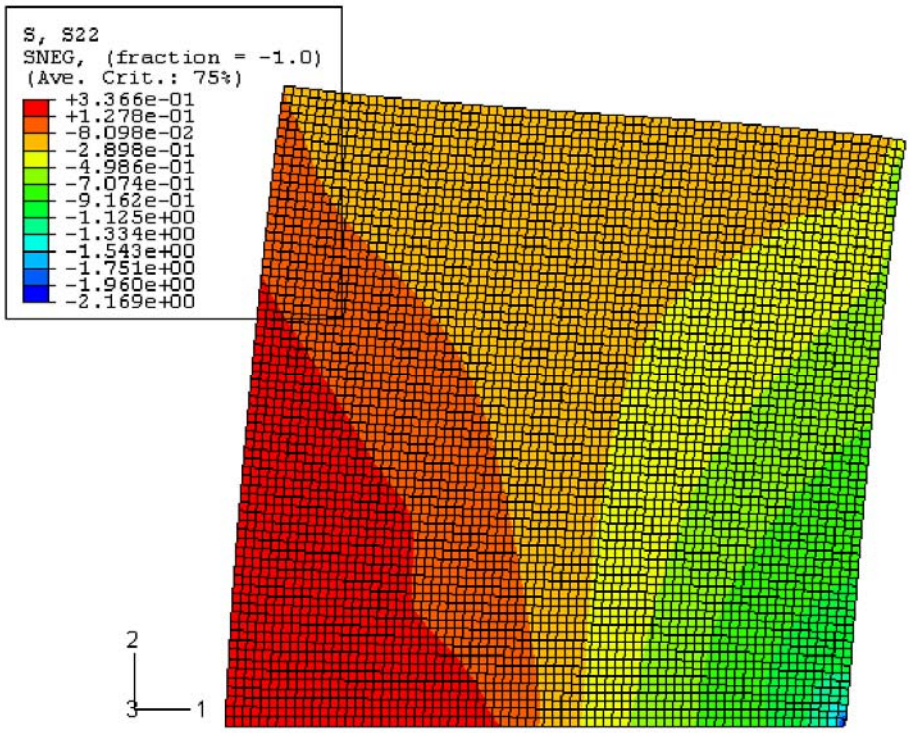

Figure (4.18) Vertical stress distribution in wall fixed at base only

4.7.5.2 Two-Layer Carbon Laminates on One Side of a Wall Fixed at Base Only:

In this specimen the wall failed at a load of 25 kips compared to the other specimen which was restrained for displacement in the Z-direction and the rotation around X and Y axes and failed at 100 kips; the adopted model is very sensitive to asymmetry.

4.7.5.3 One-Layer Carbon Laminate on Two Sides of a Wall Fixed at Base Only:

In this specimen the wall failed at the same load level (100 kips) like the other specimen which was restrained in the Z- direction and the rotation around the X and Y axes. This is due to the fact that the laminates on both side of the wall imposed an out-of-plane restraining action.

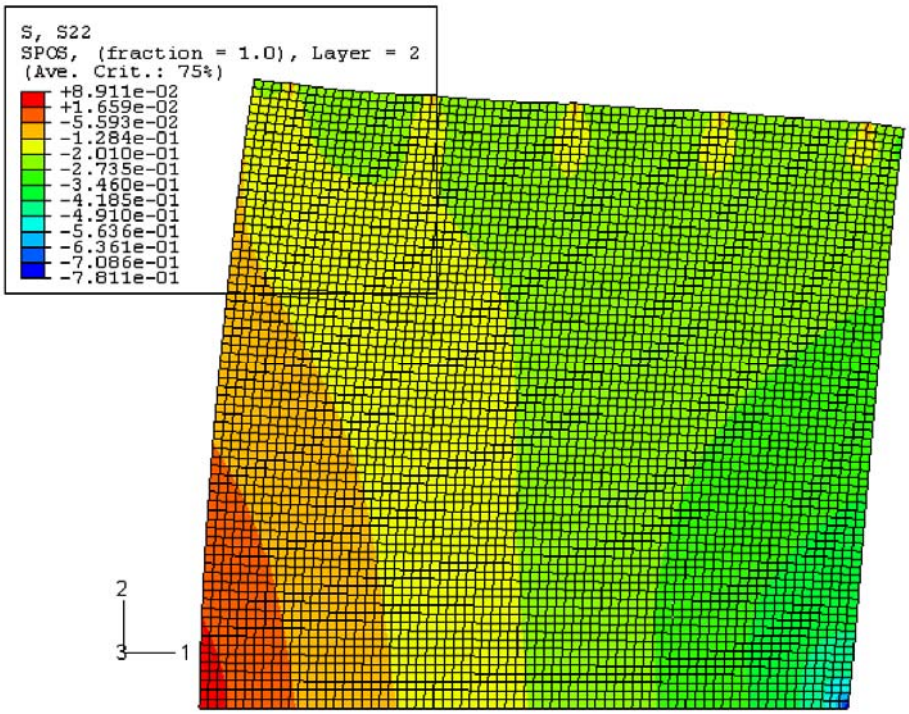

Figure (4.19) Stress in the Y-direction in wall retrofitted by 2-layer carbon laminates on one side and fixed at base only

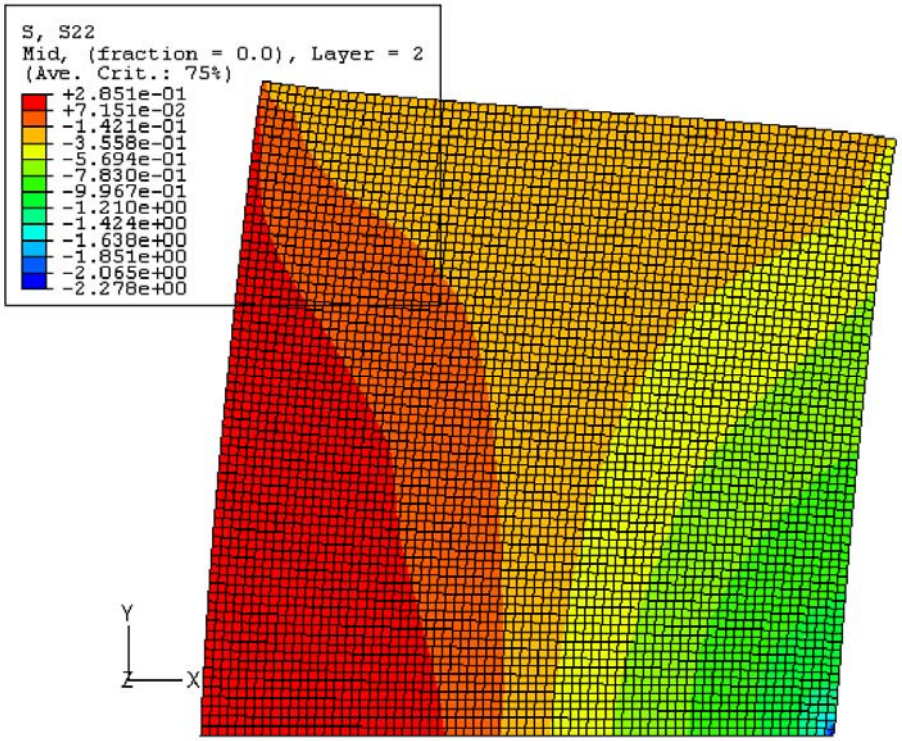

Figure (4.20) Stress in the Y-direction in wall retrofitted by one layer carbon laminate on each side and fixed at base only

CHAPTER 5

WALLS WITH DIFFERENT FRP STRENGTHENING FORMS

5.1 Summary of Analyzed FRP Strengthened Walls

In this chapter the performance of the FRP strengthened walls which were tested experimentally by Allam (2002) is evaluated, and the results were compared to the experimental values. In addition, other strengthening schemes are also evaluated by the software.

In all analyses, a uniform mesh size of 1x1 inch with a thickness of six inches, using an elastic material of an average modulus of elasticity of 950 Ksi, is examined. All walls are reinforced with steel and strengthened by one of the FRP schemes.

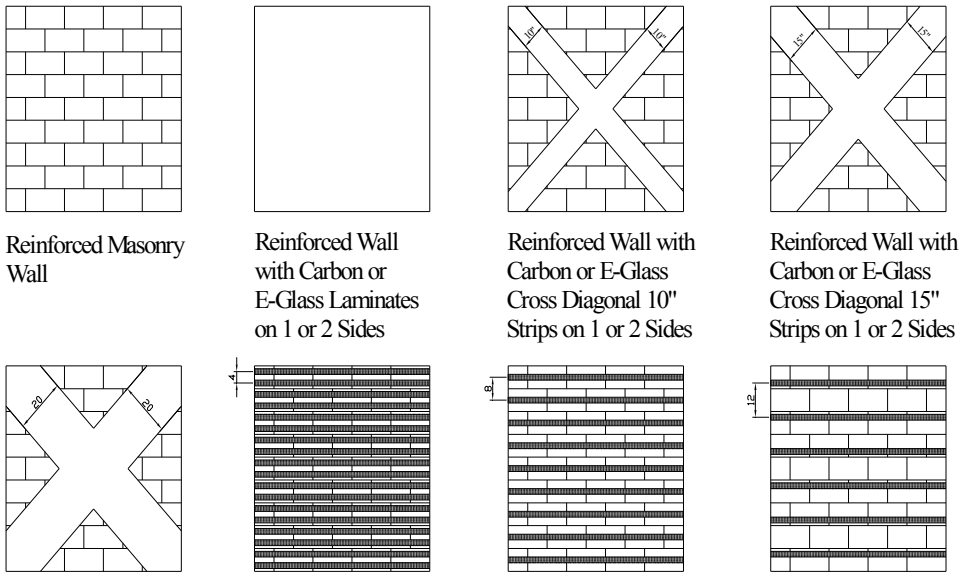

Figure (5.1) Wall specimens under study

5.2 Walls Strengthened with Carbon Laminates

In this case, all walls are fully covered with carbon laminates. At first, one layer of carbon/epoxy laminate was added to the wall from one side only and this is compared to the virgin wall with steel and no laminates. The wall failed at a load level of 95 kips with a deflection of 0.139 inch. The distribution of vertical stress is displayed in Figure (5.2).

Next, emphasis is placed on a wall with double sided carbon/epoxy retrofit to investigate the strengthening effect. In this specimen, the wall failed at a load level of 100 kips with a deflection of 0.137 inch. This was expected in comparison to the wall retrofitted from one side only; here it can be seen that the failure load has increased and the deformation has decreased. The distribution of the vertical stress was identical to that shown in Figure (5.2) with only changes in the values of the stress.

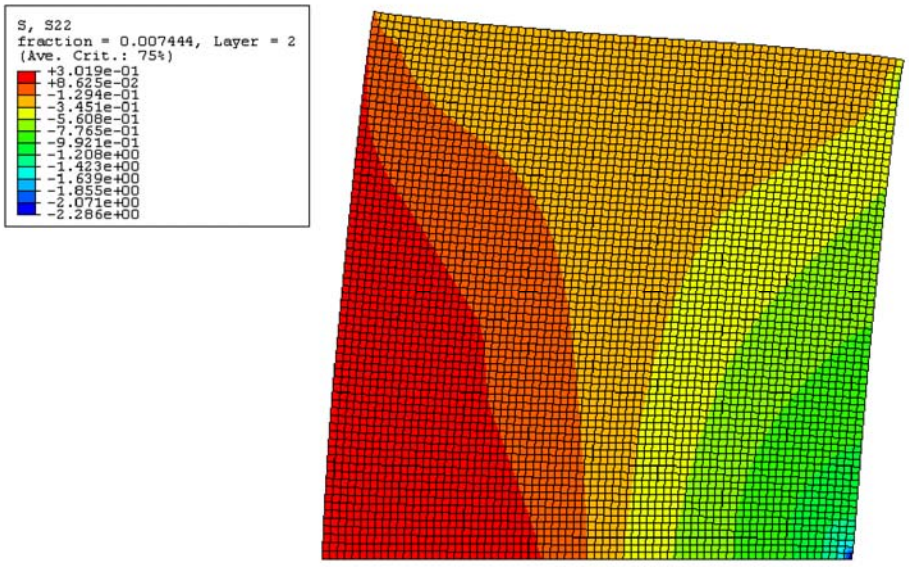

Figure (5.2) Distribution of vertical stress for a wall with one layer of carbon laminate on one side only

When the wall was retrofitted with two layers of carbon laminates on one side only, it failed at an identical load level of 100 kips with a deflection of 0.137 inch; these are the same results for the wall with one layer carbon laminate on each side. This is also expected in the model as the joint restraints imposed on the wall do not allow the wall to move in the Z-direction or to rotate about the X- or Y- axis.

Finally, the effect of adding more FRP layers was investigated by placing two layers of carbon laminates on each of the two sides of the wall. In this specimen, the failure load increased to 110 kips. Such a load was the highest of all specimens examined in this study (Figure 5.3).

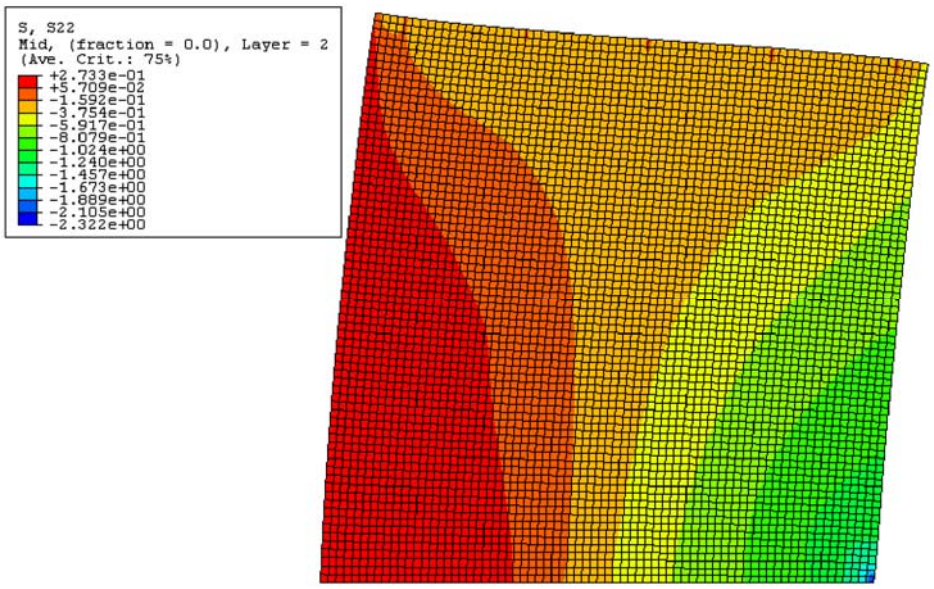

Figure (5.3) Distribution of vertical stress for a wall with two layers of carbon laminates on each of the two sides

5.3 Walls Strengthened with Glass Laminates

The main objective of using the E-glass laminates is to demonstrate the effectiveness of E-glass in retrofitting the masonry wall compared to the carbon laminates which are much more expensive.

The same routine was applied to the walls strengthened with E-glass as those strengthened with carbon laminates. At first, with one layer on one side only, the wall failed at a load level of 90 kips with a deflection of 0.140 inch. As expected, the wall failed at a lower load level when retrofitted with E-glass laminate than with carbon laminate due to the fact that the E-glass laminate has much lower modulus of elasticity and tensile strength than the carbon laminate.

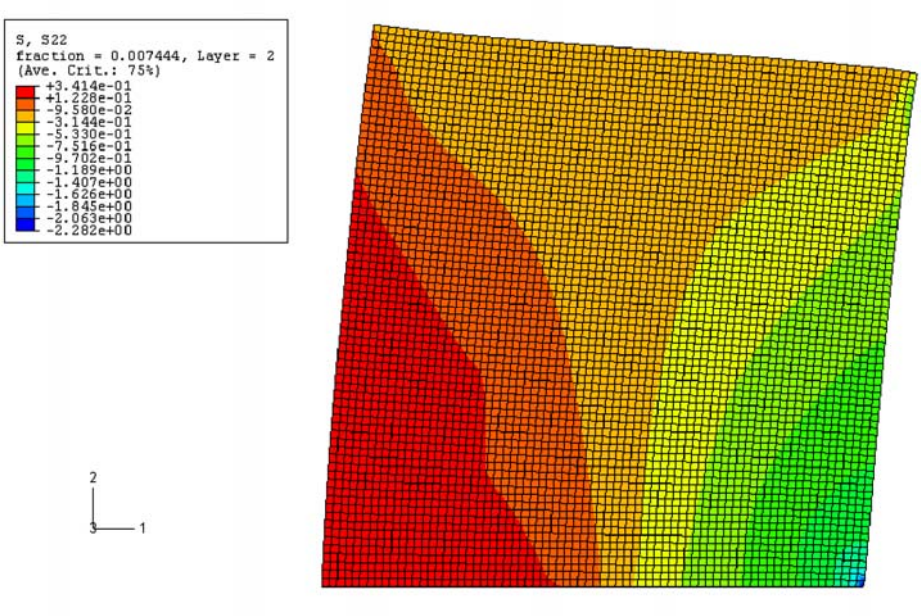

Figure (5.4) Distribution of vertical stress for a wall with one layer of E-glass laminate on one side only

When an additional layer of E-glass was placed on the other side of the wall, the wall failed at a load level of 90 kips. Here the use of an extra layer of E-glass laminate did not increase the failure load; however, it reduced the global displacement of the wall as the extra laminate imposed a restraining effect on the wall.

When two layers were placed on each side of the wall (Figure 5.5), it failed at a load level of 95 kips with a deflection of 0.139 inch. Here the use of two layers on each side increased the failure load; however, it did not reach the load at which the

same specimen with carbon laminates failed. This is due to the fact that the carbon laminates are much stronger than the E-glass laminates.

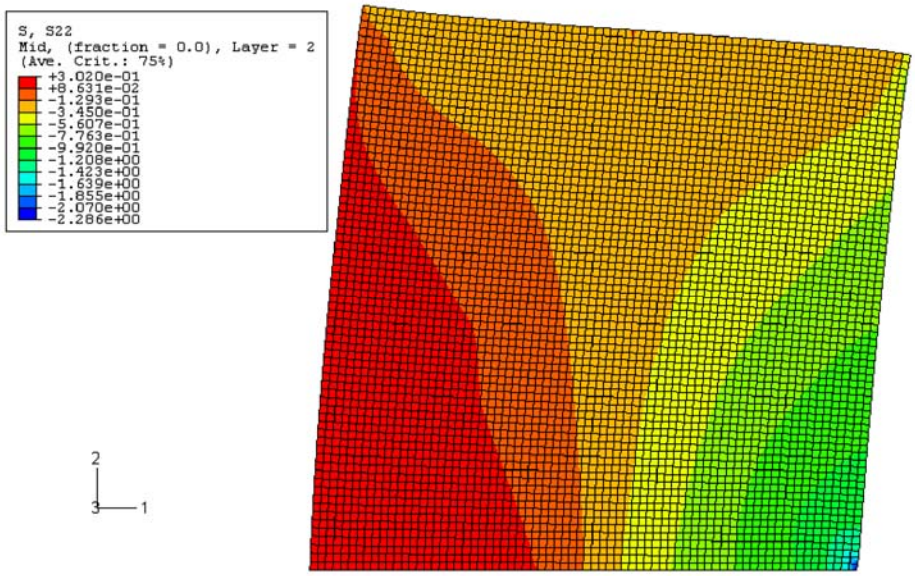

Figure (5.5) Distribution of vertical stress for a wall with two layers of E-glass laminates on each of the two sides

5.4 Walls Strengthened with Horizontal Precured Carbon Strips

Precured carbon strips may be placed on one or two sides of the wall, and the distance center to center between strips may vary as well.

At first, the strips were placed on one side only at a spacing of four inches on center. The specimen failed at a load level of 90 kips with a deflection of 0.139 inch (Figure 5.6). This specimen was expected to fail at a higher load than the specimen with one layer carbon laminate on one side, since the carbon strips are stronger than the carbon laminates. This was not realized possibly because the carbon strips did not cover the entire wall which may have resulted in early failure in the uncovered parts of the masonry.

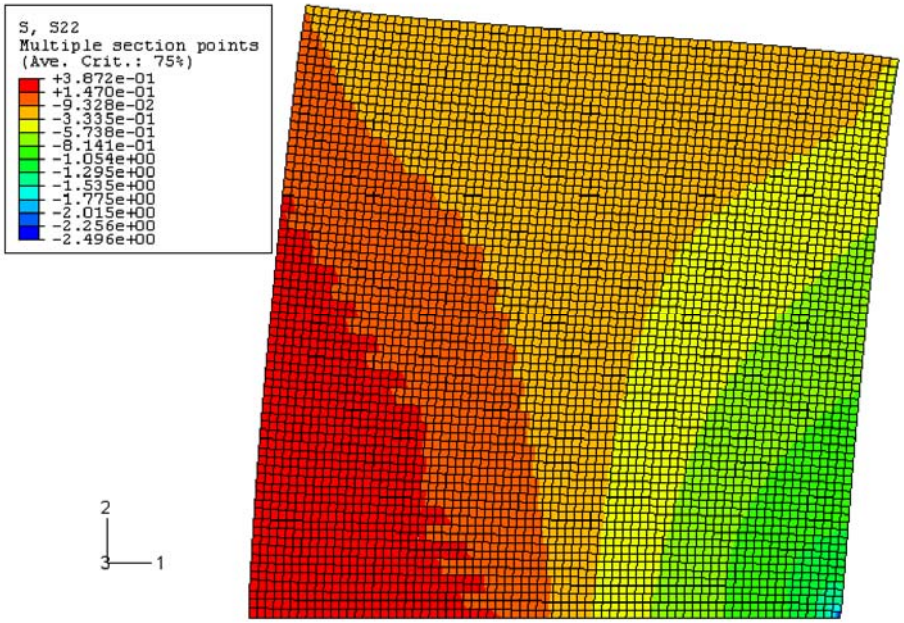

Figure (5.6) Distribution of vertical stress for a wall with 2-inch horizontal carbon strips spaced at 4 inch on center on one side only

When the spacing between the strips was increased to 8-inch on center, the wall failed at a load level of 85 kips. The distribution of the vertical stress in the wall in this case is shown in Figure (5.7). The load level at which the wall failed is the same load level at which the unretrofitted wall failed. However, the displacement of the retrofitted wall is lower than the unretrofitted wall at the same failure load, which implies that retrofitting may only result in a decrease of the deformation of the wall.

When the spacing was further increased to 12 inches, the failure load remained at 85 kips with slight increase in the displacement than the case when 8-inch spacing was used.

It is clear that the 4-inch spacing on center between the strips was optimal. Further, placing the strips on both sides of the wall did not substantially increase the failure load. Again, this may be attributed to the local failure mode of the masonry blocks.

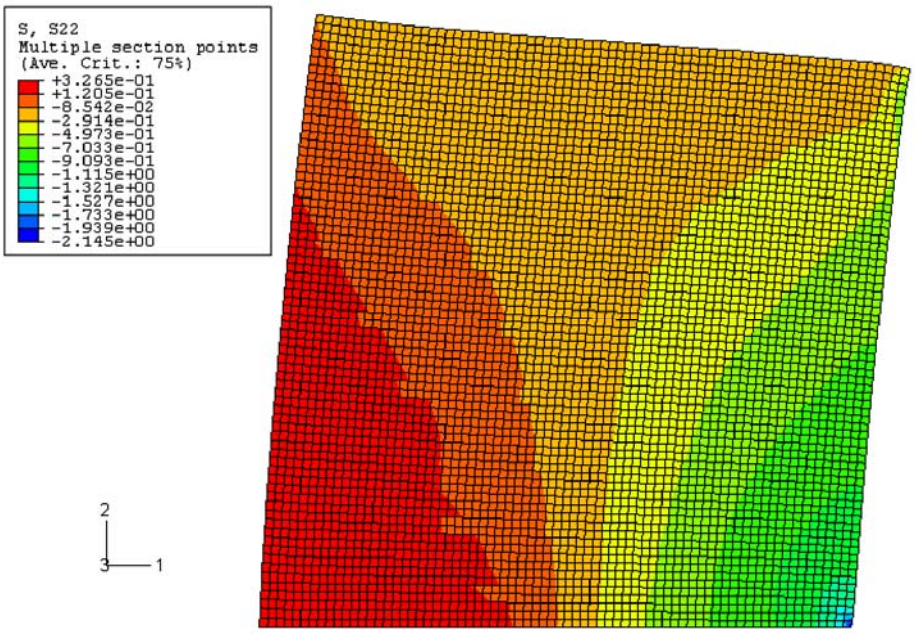

Figure (5.7) Distribution of vertical stress for a wall with 2-inch horizontal carbon strips spaced at 8 inch on center on one side only

5.5 Walls Strengthened with Cross Diagonal Carbon Laminates

In the last attempted retrofit technique, the wall was retrofitted with cross diagonal carbon laminates of varied width. The objective of the cross diagonal orientation of the laminates on the wall is to save the FRP material. This orientation concentrates the retrofitting on the two diagonals of the wall where shear failure may take place.

In the first specimen, one layer of cross diagonal carbon laminates of ten inch width was placed on one side only. In this specimen, the wall failed at a load level of 90 kips with a deflection of 0.138 inch (Figure 5.8). This means that the cross diagonal orientation is not as effective as when the whole wall is covered, yet it has an apparent strengthening effect on the wall with reduced material consumption.

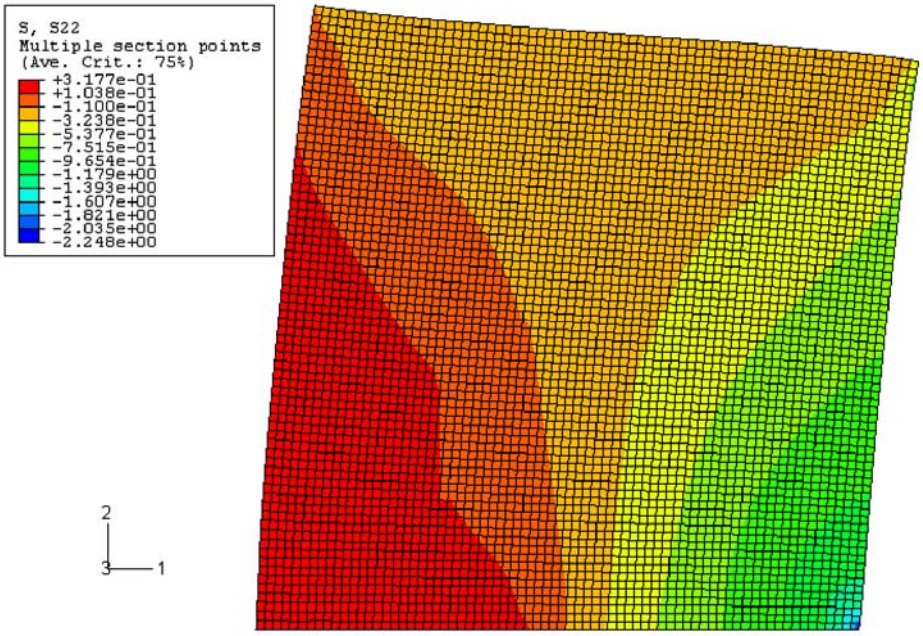

Figure (5.8) Distribution of vertical stress for a wall with one layer, 10-inch wide cross diagonal laminate on one side only

When the width of the diagonal laminates was increased to 15 inch and 20 inch, the corresponding failure loads changed very little, indicating that this method of retrofit was not suitable for this type of composition and configuration of the wall. This was further illustrated when e-glass laminates were used. The failure load remained at 85 kips which is the same as the failure load of the unretrofitted wall.

CHAPTER 6

CONCLUSIONS AND RECOMMENDATIONS

6.1 Conclusions

Based on the outcome of the present theoretical study and the review of the literature, it can be concluded that:

- Design formulae available for predicting the lateral load capacity of FRP strengthened concrete masonry walls provide capacity levels much higher than observed experimentally from tests conducted on full-scale wall samples under cyclic lateral loads.
- The discrepancy between the capacities predicted by the design formulae and those observed experimentally is attributed to the occurrence of a limiting failure mode, not accounted for in the design formulae, due to premature compression failure of the masonry units at the wall toe.
- A simple finite element model, which can be readily used by practicing engineers, was devised in this study to predict accurate levels of design capacities for FRP strengthened masonry walls subjected to lateral loading.
- The numerical model is only sophisticated enough to provide the necessary basic information required for design purposes.
- The finite element model of the masonry wall was devised using the software package ABACUS/STANDARD in which a layered shell element was employed to allow the modeling of the masonry in addition to the FRP laminates or strips.
- The analysis was performed under constant vertical gravity load with monotonically increasing lateral loads until wall failure.

- Appropriate mesh sizes, boundary conditions, restraints, modeling of steel reinforcement, and the no-compression criterion for the laminates were selected and their effects on the accuracy of the model were illustrated.
- Comparison between the numerical lateral loads at failure of the walls with those observed experimentally, for the different strengthening models that were tested in the laboratory, consistently confirmed the validity of the theoretical model.
- For other FRP retrofit techniques, the model also predicted the same premature failure mode.

In essence, the simple finite element model provided lateral capacities that are most consistent with the experimentally observed values, yet significantly lower than those predicted by the design formulae currently in use by practicing engineers.

6.2 Recommendation for Future Work

- Given the observed premature failure, it is recommended to develop optimized techniques to enhance the properties of masonry at the wall toes. One such a simple technique may be the application of an FRP U-laminate at the bottom ends and through the thickness of the wall. For field applications, a slit can be made at the ends of the walls for about 1 to 2 feet (0.3 to 0.6 meters) above the footing or the floor level, where a thin wet lay-up laminate can be applied in a U-shape on both sides of the wall and through the wall thickness. In order to validate this concept, both experimental and analytical studies should be conducted.
- The development of the finite element model in this study was limited by its objective, i.e., the model needed only to be sophisticated enough to provide the basic information needed for design purposes. However, a more sophisticated model taking into consideration the three-dimensional nature of the problem, especially when the FRP retrofit system is not symmetric with respect to the wall

axis, the nonlinear characteristics of the different elements such as mortar, masonry, grout, and the cyclic nature of the loading, could all be further investigated.

REFERENCES

1. Allam, K.H., In-plane Cyclic Behavior of Concrete Masonry Walls Enhanced by Advanced Composite Laminates, Masters Thesis, University of California, Irvine, California, USA, 2002.
2. Avramidou, N., Drdacky M.F., and Prochazka, P.P., Strengthening Against Damage of Brick Walls by Yarn Composites, Proceedings of the 5th International Conference on Inspection, Appraisal, Repairs & Maintenance of Buildings & Structures, Melbourne, Australia, December1999.
3. Badoux, M., Elgwady, A.M., and Lestuzzi, P., Earthquake Simulator Tests on Unreinforced Masonry Walls Before and After Upgrading with Composites, Proceedings of the 12th European Conference on Earthquake Engineering, September 2002.
4. Drysdale, R.G., Hamid, A.A., and Baker, L.R., Masonry Structures Behavior and Design, The Masonry Society, Boulder, Colorado, 1999.
5. Ehsani, M.R., Saadatmanesh, H., and Al-Saidy, A., Shear Behavior of URM Retrofitted with FRP Overlays, Journal of Composites for Construction, Vol. 1, No. 1, 1997, pp. 17-25.
6. Ehsani, M.R., and Saadatmanesh, H., Seismic Retrofit of URM Walls with Fiber Composites, The Masonry Society Journal, Vol. 14, No. 2, 1996, pp. 63-72.
7. Elgwady, A.M., Lestuzzi, P., and Badoux, M., Dynamic In-plain Behavior of URM Wall Upgraded with Composites, Proceedings of the 3rd ICCI, San Francisco, USA, 2002.
8. El-Hashimy, A., Ghanem, G.M., Abd Elnaby, S.F., and Salama, A.E., Retrofitting of Masonry Walls with Return, Proceedings of International Conference on Materials, Citadel, Ottawa, Canada, June 1997.

9. Fam, A., Musiker, D., and Rizkalla, S., In-Plane Testing of Damaged Masonry Wall Repaired with FRP, Advanced Composites Letters, Vol. 11, No. 6, 2002.
10. Ghanem, G., A. Zeid, M., and Salama, A.E., Repair and Strengthening of Masonry Assemblages Using Fiber Glass, Proceedings of 10th International Brick and Block Masonry Conference, Calgary, Canada, July 1994.
11. Holberg, A.M., and Hamilton, H.R., Repair of Concrete Masonry Block Walls Using Carbon Fiber, Montreal, Canada, 1996.
12. ICBO Evaluation Services, Inc., Acceptance Criteria for Concrete and Reinforced and Unreinforced Masonry Strengthening Using Fiber Reinforced Polymer (FRP) Composite System, AC 125, Whittier, California, January 2001.
13. Khalaf, F.M., Hendry, A.W., and Fairbairn, D.R., Study of the Compressive Strength of Blockwork Masonry, ACI Structural Journal, Vol. 91, No. 4, 1994, pp. 367-375.
14. Liu, Y., and Dawe, J.L., Analytical Modeling of Masonry Load-Bearing Walls, Canadian Journal of Civil Engineering, Vol. 30, 2003, pp. 795 – 806.
15. Marshall, O.S., and Sweeney, S.C., In-Plane Shear Performance of Masonry Walls Strengthened with FRP, Proceedings of the 47th International SAMPE Symposium, May 2002.
16. Nanni, A., and Tumialan G., Fiber-Reinforced Composites for Strengthening of Masonry Structures, Structural Engineering International, Vol. 13, No. 4, 2003, pp. 271- 278.
17. Paulay, T., and Priestley, M. J. N., Seismic Design of Reinforced Concrete and Masonry Buildings, John Wiley & Sons, 1992.

18. Sayed-Ahmed, E.Y., and Shrive, N.G., Nonlinear Finite-Element Model of Hollow Masonry, Journal of Structural Engineering, Vol. 122, No. 6, 1996, pp. 683 - 690.

19. Shing, P.B., Noland, J.L., Klamerus, E., and Spach, H., Inelastic Behavior of Concrete Masonry Shear Walls, Journal of Structural Engineering, Vol. 115, No. 9, 1989, pp. 2204-2225.

20. Shrive, N.G., Use of Fiber Reinforced Polymers to Improve Seismic Resistance of Masonry, Proceedings of SISMICA 2004 - 6° Congresso Nacional De Sismologia e Engenharia Sismica, 2004.

21. Tomaževič, M., and Lutman, M., Seismic Behavior of Masonry Walls: Modeling of Hysteretic Rules, Journal of Structural Engineering, Vol. 122, No. 9, 1996, pp. 1048-1054.

22. Tomaževič, M., and Weiss, P., Seismic Behavior of Plane and Reinforced Masonry Buildings, Journal of Structural Engineering, Vol. 120, No. 2, 1994, pp. 323-338.

23. Zaho, T., Zhang, C. J., and Xie, J., Study and Application on Strengthening the Cracked Brick Walls with Continuous Carbon Fiber Sheet, Proceedings of 1st International Conference on Advanced Polymer Composites for Structural Applications in Construction, Southampton University, Southampton, UK, April 2002, pp. 309-316

24. Zhuge, Y., and Thambiratnam, D., Nonlinear Dynamic Analysis of Unreinforced Masonry, Journal of Structural Engineering, Vol. 124, No. 3, 1998, pp. 270 - 277.